A&A 536, A16 (2011)
DOI: 10.1051/0004-6361/201116454
© ESO 2011

Astronomy & Astrophysics
Special feature

*Planck early results*

# *Planck* early results. XVI. The *Planck* view of nearby galaxies⋆

Planck Collaboration: P. A. R. Ade[71], N. Aghanim[47], M. Arnaud[58], M. Ashdown[56,4], J. Aumont[47], C. Baccigalupi[69], A. Balbi[27], A. J. Banday[74,7,63], R. B. Barreiro[53], J. G. Bartlett[3,54], E. Battaner[76], K. Benabed[48], A. Benoît[46], J.-P. Bernard[74,7], M. Bersanelli[24,40], R. Bhatia[5], J. J. Bock[54,8], A. Bonaldi[36], J. R. Bond[6], J. Borrill[62,72], F. R. Bouchet[48], M. Bucher[3], C. Burigana[39], P. Cabella[27], J.-F. Cardoso[59,3,48], A. Catalano[3,57], L. Cayón[17], A. Challinor[50,56,9], A. Chamballu[44], R.-R. Chary[45], L.-Y Chiang[49], P. R. Christensen[66,28], D. L. Clements[44], S. Colombi[48], F. Couchot[61], A. Coulais[57], B. P. Crill[54,67], F. Cuttaia[39], L. Danese[69], R. D. Davies[55], R. J. Davis[55], P. de Bernardis[23], G. de Gasperis[27], A. de Rosa[39], G. de Zotti[36,69], J. Delabrouille[3], J.-M. Delouis[48], F.-X. Désert[42], C. Dickinson[55], H. Dole[47], S. Donzelli[40,51], O. Doré[54,8], U. Dörl[63], M. Douspis[47], X. Dupac[31], G. Efstathiou[50], T. A. Enßlin[63], F. Finelli[39], O. Forni[74,7], M. Frailis[38], E. Franceschi[39], S. Galeotta[38], K. Ganga[3,45], M. Giard[74,7], G. Giardino[32], Y. Giraud-Héraud[3], J. González-Nuevo[69], K. M. Górski[54,78], S. Gratton[56,50], A. Gregorio[25], A. Gruppuso[39], F. K. Hansen[51], D. Harrison[50,56], G. Helou[8], S. Henrot-Versillé[61], D. Herranz[53], S. R. Hildebrandt[8,60,52], E. Hivon[48], M. Hobson[4], W. A. Holmes[54], W. Hovest[63], R. J. Hoyland[52], K. M. Huffenberger[77], A. H. Jaffe[44], W. C. Jones[16], M. Juvela[15], E. Keihänen[15], R. Keskitalo[54,15], T. S. Kisner[62], R. Kneissl[30,5], L. Knox[19], H. Kurki-Suonio[15,34], G. Lagache[47], A. Lähteenmäki[1,34], J.-M. Lamarre[57], A. Lasenby[4,56], R. J. Laureijs[32], C. R. Lawrence[54], S. Leach[69], R. Leonardi[31,32,20], M. Linden-Vørnle[11], M. López-Caniego[53], P. M. Lubin[20], J. F. Macías-Pérez[60], C. J. MacTavish[56], S. Madden[58], B. Maffei[55], D. Maino[24,40], N. Mandolesi[39], R. Mann[70], M. Maris[38], E. Martínez-González[53], S. Masi[23], S. Matarrese[22], F. Matthai[63], P. Mazzotta[27], A. Melchiorri[23], L. Mendes[31], A. Mennella[24,38], M.-A. Miville-Deschênes[47,6], A. Moneti[48], L. Montier[74,7], G. Morgante[39], D. Mortlock[44], D. Munshi[71,50], A. Murphy[65], P. Naselsky[66,28], P. Natoli[26,2,39], C. B. Netterfield[13], H. U. Nørgaard-Nielsen[11], F. Noviello[47], D. Novikov[44], I. Novikov[66], S. Osborne[73], F. Pajot[47], B. Partridge[33], F. Pasian[38], G. Patanchon[3], M. Peel[55], O. Perdereau[61], L. Perotto[60], F. Perrotta[69], F. Piacentini[23], M. Piat[3], S. Plaszczynski[61], E. Pointecouteau[74,7], G. Polenta[2,37], N. Ponthieu[47], T. Poutanen[34,15,1], G. Prézeau[8,54], S. Prunet[48], J.-L. Puget[47], W. T. Reach[75], R. Rebolo[52,29], M. Reinecke[63], C. Renault[60], S. Ricciardi[39], T. Riller[63], I. Ristorcelli[74,7], G. Rocha[54,8], C. Rosset[3], M. Rowan-Robinson[44], J. A. Rubiño-Martín[52,29], B. Rusholme[45], M. Sandri[39], G. Savini[68], D. Scott[14], M. D. Seiffert[54,8], P. Shellard[9], G. F. Smoot[18,62,3], J.-L. Starck[58,10], F. Stivoli[41], V. Stolyarov[4], R. Sudiwala[71], J.-F. Sygnet[48], J. A. Tauber[32], L. Terenzi[39], L. Toffolatti[12], M. Tomasi[24,40], J.-P. Torre[47], M. Tristram[61], J. Tuovinen[64], M. Türler[43], G. Umana[35], L. Valenziano[39], J. Varis[64], P. Vielva[53], F. Villa[39], N. Vittorio[27], L. A. Wade[54], B. D. Wandelt[48,21], D. Yvon[10], A. Zacchei[38], and A. Zonca[20]

*(Affiliations can be found after the references)*

Received 7 January 2011 / Accepted 10 June 2011

**ABSTRACT**

The all-sky coverage of the *Planck* Early Release Compact Source Catalogue (ERCSC) provides an unsurpassed survey of galaxies at submillimetre (submm) wavelengths, representing a major improvement in the numbers of galaxies detected, as well as the range of far-IR/submm wavelengths over which they have been observed. We here present the first results on the properties of nearby galaxies using these data. We match the ERCSC catalogue to IRAS-detected galaxies in the Imperial IRAS Faint Source Redshift Catalogue (IIFSCz), so that we can measure the spectral energy distributions (SEDs) of these objects from 60 to 850 $\mu$m. This produces a list of 1717 galaxies with reliable associations between *Planck* and IRAS, from which we select a subset of 468 for SED studies, namely those with strong detections in the three highest frequency *Planck* bands and no evidence of cirrus contamination. The SEDs are fitted using parametric dust models to determine the range of dust temperatures and emissivities. We find evidence for colder dust than has previously been found in external galaxies, with $T < 20$ K. Such cold temperatures are found using both the standard single temperature dust model with variable emissivity $\beta$, or a two dust temperature model with $\beta$ fixed at 2. We also compare our results to studies of distant submm galaxies (SMGs) which have been claimed to contain cooler dust than their local counterparts. We find that including our sample of 468 galaxies significantly reduces the distinction between the two populations. Fits to SEDs of selected objects using more sophisticated templates derived from radiative transfer models confirm the presence of the colder dust found through parametric fitting. We thus conclude that cold ($T < 20$ K) dust is a significant and largely unexplored component of many nearby galaxies.

**Key words.** galaxies: photometry – submillimeter: galaxies – infrared: galaxies – galaxies: ISM

## 1. Introduction

Dust is an important constituent of the interstellar medium (ISM) of galaxies. Whilst some properties of dust in our own and very nearby galaxies can be studied through its absorption of starlight, it was the IRAS satellite that first allowed dust emission to be directly observed in large samples of external galaxies (e.g., Devereux & Young 1990). The all-sky IRAS survey at 12, 25, 60 and 100 $\mu$m in wavelength provided much new information on the properties of dust and how this relates to other aspects of galaxies and galaxy evolution. However, the strong temperature dependence of the spectral energy distribution (SED) of dust emission, combined with limited wavelength coverage, means that IRAS was relatively insensitive to dust below a temperature of ~30 K. Observations of dust in our own Galaxy by the FIRAS instrument on COBE (Reach et al. 1995) found evidence for dust at several different temperatures. This included a widespread component at 16–21 K, and another at 10–14 K associated with molecular clouds in the inner Galaxy. A third widespread colder component, at 4–7 K, was later identified with the cosmic

⋆ Corresponding author: D. L. Clements,
e-mail: d.clements@imperial.ac.uk

infrared background (CIB; Puget et al. 1996; Fixsen et al. 1998). None of these components would be detectable in external galaxies by IRAS. COBE-DIRBE observations also detected 56 external galaxies, finding an average dust temperature of 27.6 K (Odenwald et al. 1996).

Observations at longer far-infrared (FIR) or submillimetre (submm) wavelengths from the ground (e.g., Dunne et al. 2000), from space (e.g., Dale et al. 2005) or in combination (e.g., Willmer et al. 2009), have provided hints that cooler dust plays a significant role in nearby galaxies. Observations with *Herschel* of pre-selected objects (e.g., Boselli et al. 2010) provide valuable data at 250 to 500 $\mu$m, which constrain the long wavelength dust properties for specific populations. Moderate area surveys with *Herschel* (e.g., H-ATLAS Eales et al. 2010a, covering up to 550 deg$^2$ from 100 to 500 $\mu$m) provide unbiased studies of the far-IR/submm population. However, the availability of the *Planck*[1] Early Release Compact Source Catalogue (ERCSC) provides a long wavelength counterpart to IRAS, allowing us an unbiased view of the FIR-to-submm SEDs of a large sample of nearby ($z < 0.25$) galaxies. We are now, for the first time, able to examine the role of cold dust for a wide range of objects in the local Universe.

The discovery of the CIB (Puget et al. 1996; Fixsen et al. 1998) has added to the importance of our understanding of dust in galaxies. The CIB demonstrates that roughly 50% of all energy generated in the history of the Universe was absorbed by dust and reprocessed into the FIR/submm (Gispert et al. 2000). Deep surveys at 850 $\mu$m with SCUBA (e.g., Smail et al. 1997; Hughes et al. 1998; Eales et al. 2000; Coppin et al. 2006) and at nearby wavelengths with other instruments (e.g., MAMBO, AzTEC and LABOCA, Weiß et al. 2009; Austermann et al. 2010) have revealed much higher number counts than would be predicted by a non-evolving extrapolation of the local population. There must thus be very rapid evolution of the FIR/submm galaxy population, something confirmed by observations with ISO, (e.g., Dole et al. 2001) *Spitzer* (e.g., Frayer et al. 2006; Béthermin et al. 2010; Clements et al. 2010a) and BLAST (Devlin et al. 2009). *Herschel* observations have now confirmed this rapid evolution through a combination of number count (Clements et al. 2010c; Oliver et al. 2010) and luminosity function (Dye et al. 2010; Eales et al. 2010b; Dunne et al. 2011) studies. However, detailed interpretation of these results is hampered by our poor knowledge of galaxy SEDs in the 100–1000 $\mu$m range. This is demonstrated, for example, by the result that IRAS-selected galaxies and high redshift SCUBA-selected SMGs (e.g., Clements et al. 2010b) lie in separate parts of the temperature-luminosity diagram (e.g., Clements et al. 2010b; Symeonidis et al. 2009). The origin of this separation is unclear. It might represent a genuine change in dust temperature with redshift, and selection biases may be partly involved, but it could also reflect our ignorance of the full FIR/submm SED of local galaxies. By properly establishing a zero redshift baseline for the dust SEDs of typical galaxies, the *Planck* ERCSC will allow the origins of the CIB and the nature of the galaxies that contribute to it to be much better determined.

The central goals of this paper are thus twofold: to examine the properties of a large sample of local ($z < 0.25$) galaxies to establish the range of dust temperatures and other properties found locally; and thus to set the local baseline against which higher redshift studies, and especially studies of the SMGs responsible for the CIB, can be compared.

The rest of this paper is organised as follows. In Sect. 2 we give details of *Planck*'s observations of local galaxies and the ERCSC. We also discuss the results of matching ERCSC galaxies to sources observed by IRAS. In Sect. 3 we present a comparison of the ERCSC with existing data from ground-based observatories. Section 4 presents the results of fitting parametric models to the dust SEDs of ERCSC galaxies, while Sect. 5 discusses the results of physical template fitting. Finally, we draw conclusions in Sect. 6. Throughout this paper we assume a concordance cosmology, with $H_0 = 70\,\mathrm{km\,s^{-1}\,Mpc^{-1}}$, $\Omega_\Lambda = 0.7$ and $\Omega_\mathrm{M} = 0.3$.

## 2. *Planck* observations of nearby galaxies

### 2.1. The Planck mission

*Planck* (Tauber et al. 2010; Planck Collaboration 2011a) is the third generation space mission to measure the anisotropy of the cosmic microwave background (CMB). It observes the sky in nine frequency bands covering 30–857 GHz with high sensitivity and angular resolution from 31′ to 5′. The Low Frequency Instrument LFI; (Mandolesi et al. 2010; Bersanelli et al. 2010; Mennella et al. 2011) covers the 28.5, 44.1, and 70.3 GHz bands, with amplifiers cooled to 20 K. The High Frequency Instrument (HFI; Lamarre et al. 2010; Planck HFI Core Team 2011a) covers the 100, 143, 217, 353, 545, and 857 GHz bands, with bolometers cooled to 0.1 K. Polarization is measured in all but the highest two bands (Leahy et al. 2010; Rosset et al. 2010). A combination of radiative cooling and three mechanical coolers produces the temperatures needed for the detectors and optics (Planck Collaboration 2011b). Two data processing centers (DPCs) check and calibrate the data and make maps of the sky (Planck HFI Core Team 2011b; Zacchei et al. 2011). *Planck*'s sensitivity, angular resolution, and frequency coverage make it a powerful instrument for Galactic and extragalactic astrophysics as well as cosmology. Early astrophysics results are given in *Planck* Collaboration (2011h–z).

### 2.2. The Planck early release compact source catalogue

The *Planck* ERCSC (Planck Collaboration 2011c) provides positions and flux densities of compact sources found in each of the nine *Planck* frequency maps. The flux densities are calculated using aperture photometry, with careful modelling of *Planck*'s elliptical beams. The colour corrections for sources with spectral index $\alpha = -0.5$ (using the convention $S_\nu \propto \nu^\alpha$) are 1.017, 1.021 and 1.030, respectively, for the 28.5, 44.1, and 70.3 GHz LFI channels. Flux densities taken from the ERCSC should be divided by the appropriate colour correction to give the correct flux values for an assumed narrow band measurement at the central frequency. For frequencies from 28.5 to 143 GHz, compact sources have been detected using a version of the "Powell Snakes" techniques (Carvalho et al. 2009); for details see Planck Collaboration (2011c). In the four higher frequency channels, sources were located using the SExtractor package (Bertin & Arnouts 1996). Sources detected in one or more of the frequency maps were then put through a further set of secondary selection criteria; these are discussed in detail in Planck Collaboration (2011c). The primary criterion utilized

[1] *Planck* (http://www.esa.int/Planck) is a project of the European Space Agency (ESA) with instruments provided by two scientific consortia funded by ESA member states (in particular the lead countries France and Italy), with contributions from NASA (USA) and telescope reflectors provided by a collaboration between ESA and a scientific consortium led and funded by Denmark.

was a Monte Carlo assessment designed to ensure that ≥90% of the sources in the catalogue have a flux accuracy of at least 30%.

For this paper we are primarily interested in the sources selected in the 857 GHz (350 $\mu$m) band, the catalog of which also includes bandmerged fluxes for each 857 GHz detected source in the next three highest *Planck* bands i.e. 545 GHz, 353 GHz, and 217 GHz (~550 $\mu$m, 850 $\mu$m and 1300 $\mu$m respectively). The *Planck* beam is 5′ in all these bands and all sources are detected in the 857 GHz band with at least 5$\sigma$ significance. This does not translate into a single fixed flux limit, however, because of the effects of foreground extended emission and the details of the *Planck* scanning strategy which mean that some parts of the sky (e.g. the ecliptic poles) are scanned more often than others.

### 2.3. Matching the ERCSC to IRAS data

To understand the FIR Spectral SEDs we need a combination of data at long wavelengths, provided by the *Planck* ERCSC, and data near the peak of a typical galaxy dust SED at about 100 $\mu$m. The best source for the latter information is the IRAS all-sky FIR survey, and the most recent analysis of the IRAS Faint Source Catalogue (FSC) is provided by Wang & Rowan-Robinson (2009) in the Imperial IRAS FSC redshift survey (IIFSCz). This was constructed using IRAS FSC sources, all of which are at $|b| > 20°$, with IRAS colours used to exclude stars and cirrus sources (with $S(100)/S(60) > 8$). The NASA Extragalactic Database (NED) was then used to find spectroscopic redshifts for the resulting FSC source list, and to associate the sources with SDSS (where available; York et al. 2000) and 2MASS (Skrutskie et al. 2006) galaxies to find photometry at 0.36–2.2 $\mu$m. This photometry was then used to estimate photometric redshifts for sources without spectroscopic redshifts. A full description of the photometric method used and the accuracies obtained for this work is included in Wang & Rowan-Robinson (2009).

The starting point for matching the ERCSC to the IIFSCz is the set of 9042 sources detected at 857 GHz (350 $\mu$m) by *Planck*. This is then restricted to the 5773 sources at $|b| > 20°$ for which there will be FSC data. Associations of ERCSC sources with IIFSCz were looked for using a search radius of 5′. The histogram of positional offsets is shown in Fig. 1. The bulk of associations have offsets within 2′. Even at 5′ there is no steep increase in the number of associations which would be indicative of a large fraction of chance associations. On the basis of source surface-density, the chance of a random association with an IIFSCz source within 3′ is 1.6%, and within 5′ it is 4.5%. A total of 1966 associations were found within 5′. There were 106 cases where an ERCSC source picked up an association with more than one IIFSCz source within 5′. We examined these cases carefully to ensure that only a single association was accepted. Generally the nearer association was preferred. Where the offsets of the two associations were comparable, the brighter IRAS source was preferred. There are 20 cases where two bright galaxies less than 5′ apart have generated a single ERCSC source, for which there may be a significant contribution from both galaxies to the ERCSC flux. These confused sources would benefit from additional observations with ground-based submm instruments to determine the contribution of each component to the submm emission detected by *Planck*.

The remaining ERCSC-IIFSCz associations were further scrutinised as follows. Firstly, for sources with positional offsets between the two catalogues in the range 3–5′ all NED associations within 5′ of the ERCSC positions were examined to test the validity of the association with the IRAS source. This included

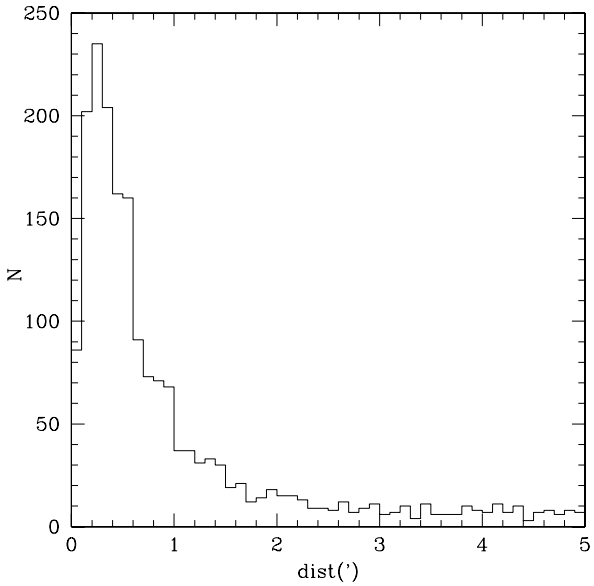


**Fig. 1.** Histogram of offsets between ERCSC and IIFSCz positions.

inspection of the Sky Survey postage stamps provided in NED. Associations were accepted as real if the associated galaxy had a blue ($g$ or $B$) magnitude brighter than 16. The surface-density of such galaxies leads to the probability of a chance association being ~3%. For sources where there was both an IRAS and a 2MASS association, this limit was relaxed to $B = 17$ (or $K \sim 13$). Of the 88 ERCSC-IIFSCz associations with positional offsets 3–5′ (and with spectroscopic or photometric redshifts) 72 were associated with bright galaxies, two were associated with a second FSC source having cirrus-like colours and are presumed to be cirrus, and the remaining 14 are classified as possible galaxy associations (these are excluded from the reliable galaxy catalogue used here for further analysis).

The second category of ERCSC-IIFSCz associations which we scrutinised in detail were those for which there is no redshift in the IIFSCz. There were 165 of these and the NED associations suggest that 38 are bright galaxies, seven are cirrus, two are bright planetary nebulae, and the remaining 118 are classified as possible galaxy associations (and excluded here). We were left with 1717 reliable ERCSC-IIFSCz galaxy associations of which 337 are flagged as extended in the ERCSC. 1597 of these 1717 objects have spectroscopic redshifts. None of the sources with photometric-only redshifts or possible multiple identifications are used in the subsequent SED analyses in this paper.

### 2.4. ERCSC sources not associated with IIFSCz sources

Figure 2 shows the sky distribution of ERCSC sources at $|b| > 20°$, with sources flagged as extended in the ERCSC shown as blue filled hexagons, and point-sources shown in black. Associations with the IIFSCz are shown as red circles. The extended sources not associated with IIFSCz sources have a strikingly clustered distribution, which matches the areas of our Galaxy with strong cirrus emission, as evidenced by IRAS 100 $\mu$m maps and by the ERCSC cirrus flag (values >0.25). We presume the majority of these are cirrus sources and not extragalactic.

To test this further, we looked for NED associations with all 444 extended ERCSC sources lacking IIFSCz associations (i.e. are within 5′) at $|b| > 60°$. Only 12 were found to have

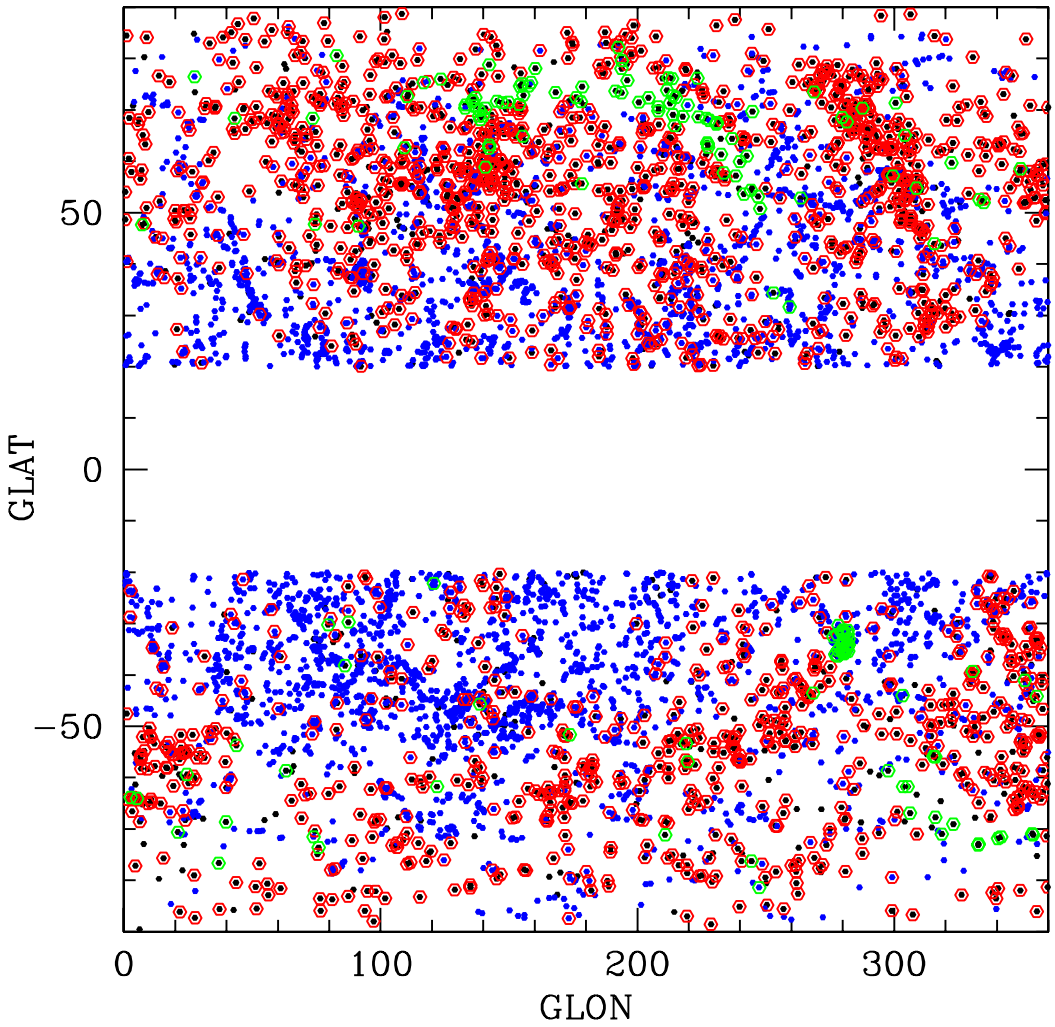


**Fig. 2.** Sky plot of ERCSC sources in galactic coordinates. Black filled hexagons are ERCSC point-sources and blue filled hexagons are ERCSC sources flagged as extended. Red hexagons are sources associated with IIFSCz IRAS FSC galaxies, after scrutinising suspect categories with NED (and excluding some, as described in the text). Green hexagons are ERCSC sources not associated with IIFSCz, but associated with bright galaxies in NED (only for $|b| > 60°$ for extended sources).

associations with bright ($b$, $g < 16$) galaxies. Extrapolating to $|b| = 20$–$60°$, we estimate that a further ~50 of these extended non-FSC sources will be bright galaxies. The remainder of the 3431 extended non-FSC sources at $|b| > 20°$ are presumed to be Galactic cirrus.

A ridge of non-FSC point sources can be seen in Fig. 2 at $b \sim 70°$, $l \sim 120$–$230°$. These correspond to one of the IRAS coverage gaps. We examined NED associations for all 482 ERCSC point-sources not associated with IIFSCz sources. 32 were found to be associated with Local Group galaxies (M 31, SMC and WLM, with 28 in the LMC), 123 are bright galaxies, 27 are associated with IRAS FSC or PSC Galactic cirrus sources, and 10 are bright stars or planetary nebulae. Most of the bright galaxies lie in the IRAS coverage gaps. The remaining 289 are classified as possible galaxy associations (and excluded here).

To summarise, we have found a net total of 1884 definite associations with galaxies. These constitute an ERCSC galaxy catalogue. A further 419 sources are not associated with bright galaxies, but there are grounds for thinking they could be extra-galactic sources. Some have IIFSCz associations, but there are too many possible faint optical or near-IR galaxy counterparts to be confident which might be associated with the ERCSC source. Some of these 419 sources are almost certainly fainter galaxies, although many could turn out to be cirrus. Improved submm or FIR positions are needed, either via *Herschel* or ground-based telescopes, to identify these sources reliably.

Following this identification analysis we restrict ourselves to those galaxies with reliable IIFSCz associations and with detections in the 857 and 545 GHz bands at significance of $5\sigma$ or greater, as well as detections in the 353 GHz band of $3\sigma$ or greater. This amounts to a total sample size of 595 galaxies.

### 2.5. Cirrus contamination

Our analysis of the non-IIFSCz-identified ERCSC sources in Sect. 2.4 led us to the conclusion that sources which are extended in the ERCSC are a result of cirrus structure in our own Galaxy, or at best are a combination of cirrus structure with flux from a galaxy. Of the 595 reliably detected IIFSCz-identified ERCSC sources, 127 are listed as extended in the ERCSC. We test these objects for the possibility of cirrus contamination by examining the amplitude of the local cirrus fluctuations in the 100 $\mu$m cirrus maps of Schlegel et al. (1998). We adopt this approach since regions of greatest cirrus fluctuation are those most likely

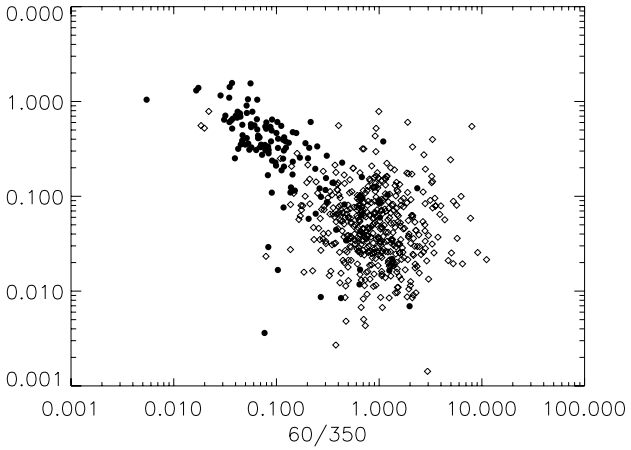


**Fig. 3.** 60 $\mu$m to 857 GHz (i.e., 350 $\mu$m) colour plotted against the cirrus RMS at 100 $\mu$m in IRAS. ERCSC sources classified as point-like are shown as open diamonds, while extended sources are shown as solid dots. Note that the extended sources show a clear correlation between colour and cirrus RMS, indicating that these sources are likely to be contaminated by cirrus emission.

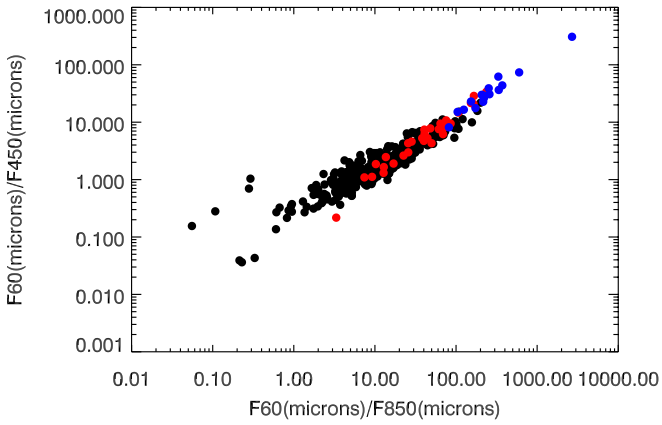


**Fig. 4.** Colours for the ERCSC galaxies (black dots) compared to those found for SLUGS galaxies (red; Dunne & Eales 2001; Vlahakis et al. 2005) and ULIRGs (blue; Clements et al. 2010b). A flux correction factor of 0.506 has been applied to the *Planck* 857 GHz (350 $\mu$m) flux densities to extrapolate them to the SCUBA 450 $\mu$m band. This correction is appropriate for sources with the SLUGS median galaxy SED i.e. $T = 35$ K and $\beta = 1.3$, but this factor will be similar for most reasonable dust SEDs. Only sources detected at >3$\sigma$ in the 353 GHz (850 $\mu$m) band and at >5$\sigma$ in the 857 GHz (350 $\mu$m) band (the requirement for inclusion in our analysis) are shown. The four points above the general trend in the lower left of the diagram are bright non-thermal dominated sources 3C 279, [HB89]0537−441, OJ+287 and 3C 273. The SLUGS point with the lowest 60 $\mu$m to SCUBA flux ratios corresponds to the galaxy IC 979; it is offset from the general correlation for SLUGS and ERCSC galaxies, and Vlahakis et al. (2005) note that its IRAS flux densities should be treated with caution.

to cause problems for point source detection in the ERCSC. We measure the cirrus RMS in a $3 \times 3$ array of points, separated by 0.1° and centred on the position of the ERCSC source. Since cirrus emission is likely to have cooler FIR-to-submm colours than the integrated emission of an external galaxy, we then look for any correlation between cirrus RMS and the 60 $\mu$m-to-857 GHz colour. We plot this relation in Fig. 3.

As can be seen from Fig. 3, there appears to be a correlation between colour and cirrus RMS for the sources classified as extended in the ERCSC. We conclude that the ERCSC fluxes for these sources are partially contaminated with cirrus emission from our own Galaxy. We thus exclude these 127 sources from further analysis. Of the remaining 468 non-extended ERCSC sources, fewer than 10 lie in the region of this correlation. These sources are retained for the following analysis, but any conclusions that come solely from these specific sources will be treated with caution.

More generally, this analysis highlights one of the issues that must be faced when using the ERCSC catalogue. Anyone wishing to cross-match *Planck* sources, especially those detected at high frequencies, with sources at other wavelengths, needs to take great care in ensuring that the ERCSC fluxes are not contaminated by cirrus emission.

## 3. Comparison to existing submm data

### 3.1. Galaxies detected with SCUBA

The largest studies of cool dust in external galaxies to date have been associated with the SCUBA Local Universe Galaxy Survey (SLUGS) and its extensions (Dunne et al. 2000; Dunne & Eales 2001; Vlahakis et al. 2005; Clements et al. 2010b). These encompass a total of about 250 objects that were observed with SCUBA. The targets were selected on the basis of IRAS flux $B$-band optical magnitude or FIR luminosity. Most of the objects were detected only at 850 $\mu$m (i.e., not also at 450 $\mu$m), allowing, with the IRAS data, only a single component $(T, \beta)$ fit – where the SED is described as $S_\nu \propto \nu^\beta B(\nu, T)$, with $B(\nu, T)$ being the *Planck* function, and the parameters $T$ and $\beta$ representing temperature and dust emissivity index, respectively. A small fraction of SLUGS galaxies were also detected at 450 $\mu$m, allowing for the existence of a second, cooler, dust component to be assessed. For these objects, and more recently for an ultraluminous IR galaxy (ULIRG) sample, Dunne & Eales (2001) and Clements et al. (2010b) found some evidence for a colder dust contribution.

The presence of colder dust can be inferred from colour-colour diagrams when two submm flux densities are available. We show the SLUGS sources and the ERCSC sources (after colour corrections to the *Planck* flux densities and a suitable scaling has been applied to convert from *Planck* 857 GHz flux density to the SCUBA 450 $\mu$m band) in Fig. 4. As can be seen, the *Planck* galaxies lie on the same broad trend as the SLUGS galaxies (with the exception of a small number of objects dominated by a non-thermal AGN component, such as 3C 273 and 3C 279). The ERCSC sources, though, extend the trend to cooler FIR/submm colours than were found for the SLUGS objects, suggesting that the galaxies detected in the ERCSC contain cooler dust than was detected in the majority of SLUGS sources.

### 3.2. CO contamination

One factor that has complicated the interpretation of ground-based submm observations of galaxies has been the presence of CO emission lines within the submm passbands that make a significant contribution to the continuum flux. Seaquist et al. (2004) estimated that the CO (3–2) line contributed an average 25% of the flux received in the SCUBA 850 $\mu$m continuum passband for galaxies observed in the SLUGS survey, with the range of flux contributions going from 10–45% for the subset of SLUGS galaxies for which CO(3–2) observations were available. The SCUBA 850 $\mu$m filter has a bandwidth of

~30 GHz. The *Planck* 353 GHz (850 $\mu$m) filter is significantly broader, at ~90 GHz, so the line contribution will be correspondingly smaller at ~8% on average. The broad *Planck* passband also means that CO(3–2) is a potential contaminant over a broader redshift range than for ground based studies, with contamination possible from $z = 0$ out to $z = 0.15$, which essentially encompasses all of the galaxies discussed in this paper. This CO contamination fraction can be checked using observed values of integrated CO 3–2 line fluxes for a variety of objects from Bayet et al. (2006) and matching them to continuum observations of similar beamsize to the CO observations. We find contamination fractions of 2% for Arp 220, 6% for Mrk 231 and a worst case example in the central region of NGC 253, where a contamination of 11% is calculated. This level of contamination in a real object is unlikely since we this tacitly assumes that the CO and continuum emission have matching spatial extent, while in a real object the continuum emission is likely to be more extended than CO, leading to a smaller fraction of CO contamination.

We can extend this analysis to other *Planck* bands using NGC 253 as a worst case since, unlike most others, this object has been observed over the full range of CO transitions accessible from the ground. We find that the higher frequency bands have a reduced level of contamination compared to the 353 channel, with <1% at 857 (350 $\mu$m) and 6% at 545 (550 $\mu$m), assuming a flat spectral line energy distribution to estimate the contribution of the CO 5–4 line that is inaccessible from the ground. More normal objects than NGC 253, not dominated by an ongoing starburst, will have an even smaller level of CO contamination than this. At lower frequencies, though, the contamination can become more serious. CO 2–1 could contribute as much as 21% of the continuum flux in the 217 band in the inner regions of NGC 253 and as much as 75% in the 100 band. The inner regions of NGC 253 are very much a worst case scenario, so more typical sources would of course suffer much less contamination. However, very few galaxies are detected by *Planck* solely in thermal emission in this band, and the few that are detected are bright nearby objects with substantial archival data that can allow a direct assessment of the CO contribution (Peel et al., in prep.).

Our conclusion from this analysis is that the CO contribution to the continuum flux is likely to be smaller than other sources of uncertainty for generic ERCSC-detected galaxies except for the small number which are detected in the 217 band. Flux excesses detected in this band alone might thus result from CO emission rather than from any putative very cold dust component.

## 4. Parametric models of dust SEDs

### 4.1. Fitting method

Given the *Planck* and IRAS flux data described in Sect. 2, with appropriate colour corrections applied to the *Planck* flux densities, we model the underlying signal in observed frequency band $\nu$ as one or more grey-body sources with flux density

$$G(\nu; T, \beta) \propto \nu^{\beta} B_{\nu}(T), \tag{1}$$

where $B_{\nu}(T)$ is the *Planck* function for blackbody flux density. We fit the data $d_{\nu}$ to one-component models of the form

$$d_{\nu} = AG[\nu(1+z); T, \beta] + n_{\nu}, \tag{2}$$

or to two-component models with a fixed $\beta = 2$ grey-body exponent (e.g. Dunne & Eales 2001),

$$d_{\nu} = A_1 G[\nu(1+z); T_1, 2] + A_2 G[\nu(1+z); T_2, 2] + n_{\nu}. \tag{3}$$

In these equations, $A$ or $A_i$ is an overall amplitude for each component, and the factor of $(1 + z)$ converts from rest-frame frequency to observed frequency for an object at redshift $z$. The noise contribution is given by $n_{\nu}$, which we model as a Gaussian with variance $\sigma_{\nu}^2$. For the *Planck* channels, the determination of the noise contribution is described in Planck Collaboration (2011c). For IRAS, the detections are classified in the IIFSCZ of Wang & Rowan-Robinson (2009) into (1) good detections, for which we take $\sigma_{\nu} = 0.1 d_{\nu}$; (2) marginal detections, for which we take $\sigma_{\nu} = 0.5 d_{\nu}$; and (3) upper limits, for which we take $\sigma_{\nu}$ derived from the reported upper limit, and $d_{\nu} = 0$. As mentioned above, we only consider sources with detections in the 857 and 545 bands at significance of at least $5\sigma$ or greater and in the 353 band of at least $3\sigma$.

Thus, the parameters of our model are some subset of the $A_i, T_i, \beta$, depending on which model we fit. We use a Bayesian Markov Chain Monte Carlo (MCMC) (e.g., Lewis & Bridle 2002; Jaynes 2003) technique to probe the parameter space; with our Gaussian noise, this is equivalent to an exploration of the $\chi^2$ surface, albeit with a nonlinear parameterization. We require a $0 \leq \beta \leq 3$ and $3\,\mathrm{K} \leq T \leq 100\,\mathrm{K}$ with a uniform prior probability between those limits (detections of very low temperatures, $T < 10\,\mathrm{K}$, are actually dominated by non-thermal emission). We adopt a uniform prior on $\ln A_i$, as it ranges over many orders of magnitude for sources of widely varying absolute luminosities and distances.

The MCMC engine first creates a 15 000-sample Markov chain, varying one parameter at a time, using this to find an approximately-orthogonal linear combination of parameters, with which a subsequent 100 000-sample chain is run. Convergence is assessed by re-running a small number of chains from a different starting point and checking for agreement to much better than one standard deviation in all parameters.

We calculate an approximation to the Bayesian evidence, or model likelihood (Jaffe 1996; Jaynes 2003) in order to compare the two-temperature and one-temperature fits. The evidence is calculated as the average of the likelihood function over the prior distribution; we approximate the likelihood as a multivariate Gaussian function of the parameters centred at the maximum-likelihood MCMC sample with covariance given by the empirical covariance of the samples (this approximation ignores the prior on the amplitude of the individual grey bodies).

In Figs. 5, 6 we show sample output from our MCMC runs for different objects and models, along with the measured SEDs and fits. For objects such as F00022-6220 in Fig. 5, if we instead perform a two-temperature fit, it prefers the amplitude of the second temperature component to be many tens of orders of magnitude below the first, and gives temperature values consistent with the one-temperature fit; this indicates, along with the approximate evidence discussed above, that a one-temperature model is strongly preferred.

### 4.2. Results from parametric fits

#### 4.2.1. Single component fits

Figure 7 shows the $T - \beta$ plane for parametric fits to all 468 reliably identified non-extended sources within the ERCSC-IIFSCz cross match whose flux densities pass our S/N ratio criteria for inclusion, together with similar single temperature parametric fits from Dunne et al. (2000) and Clements et al. (2010b). As can be seen, the *Planck* ERCSC sources overlap with the SLUGS galaxies but extend to cooler temperatures and flatter, i.e., lower $\beta$, SEDs. The median parameters for the *Planck*

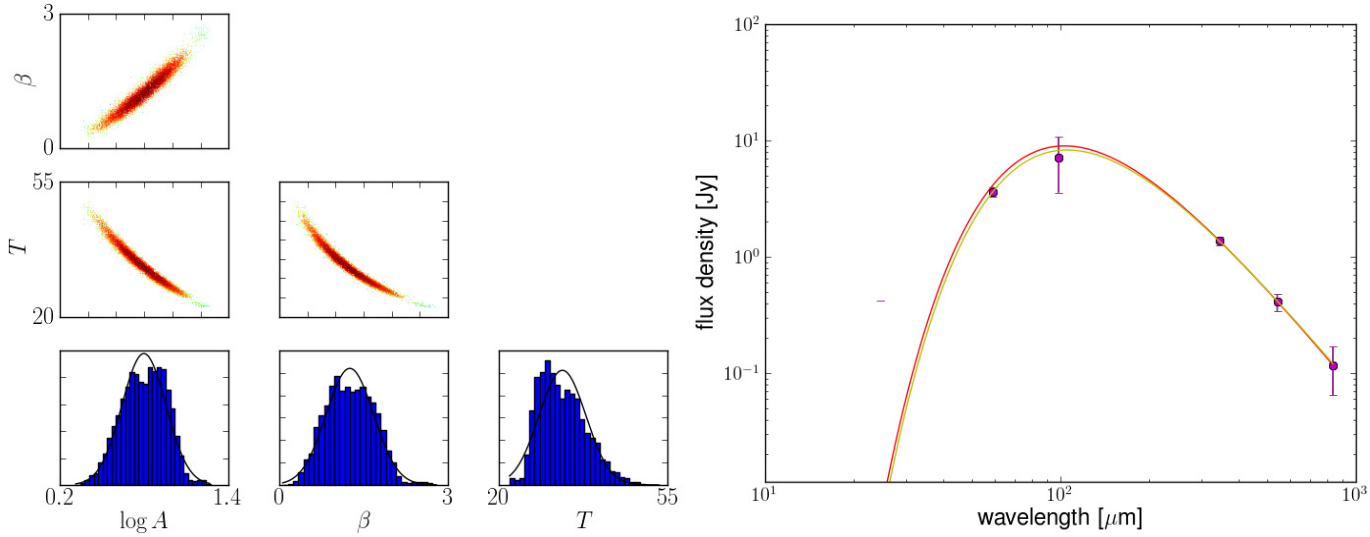


**Fig. 5.** *Left panel*: samples from the SED likelihood function ($\chi^2$) for F00022-6220 and the one-temperature model. *The bottom row* shows the one-dimensional (marginalized) posterior for the parameters ($\log A$, $\beta$, $T$), and the other panels show all two-dimensional marginal distributions. *Right panel*: the data points for this object, along with the one-temperature model for the maximum likelihood sample (yellow curve; $T = 33.0$, K, $\beta = 1.25$) and the model determined by the mean of the samples of each parameter (red curve; $T = (33.2 \pm 4.8)$ K, $\beta = 1.25 \pm 0.42$ where the errors are the standard deviations). Note the logarithmic axes which make interpretation of the error bars difficult.

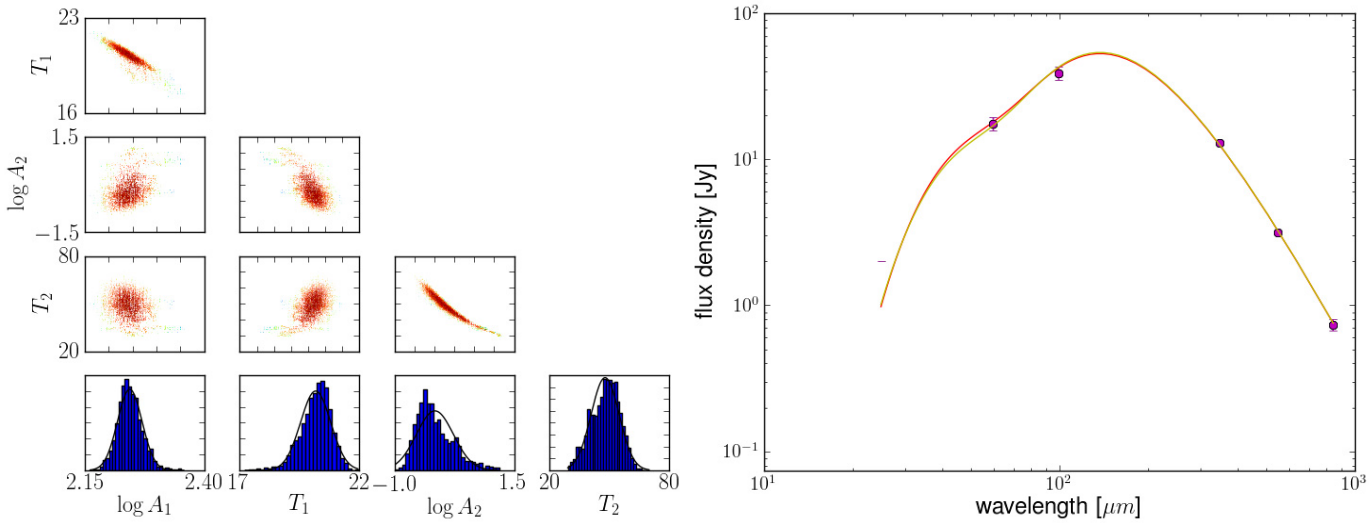


**Fig. 6.** As in Fig. 5, but for F00322-0840 and the two-temperature model with fixed $\beta = 2$. The maximum-likelihood temperatures are 20 K and 49 K the means and standard deviations are $(20 \pm 0.8)$ K and $(44 \pm 8)$ K.

sources are $T = 26.3$ K with temperatures ranging from 15 to 50 K, and $\beta = 1.2$ compared to corresponding values from 104 SLUGS galaxies Dunne et al. (2000) of $T = 35$ K and $\beta = 1.3$ and of $T = 41$ K and $\beta = 1.6$ for 26 ULIRGs Clements et al. (2010b). This confirms the result from consideration of *Planck*-IRAS colours in Fig. 4 that we are seeing cooler dust in the ERCSC-IIFSCz galaxies.

There are ten sources common to the ERCSC-IIFSCz cross-matched catalogue and the SLUGS studies. The fits using *Planck* data and using SLUGS data for all but two of these sources are in good agreement. The two exceptions are NGC 7541 and NGC 5676. The likely cause of the disagreements in these cases, is the presence of a close companion IRAS source to NGC 7541 (NGC 7537 3.1′ separation, and thus only ∼0.7 beam FWHM away), so that the *Planck* flux density is likely over-estimated, and extended IRAS emission in NGC 5676, making the IRAS FSC flux densities used in our analysis underestimates.

The position of our galaxies in the Luminosity-Temperature plane is an important question since it relates to claims of evolution in the dust properties of galaxies. It has previously been suggested that high redshift, high luminosity SMGs have lower dust temperatures and higher dust masses than more nearby objects (Yang et al. 2007). Comparison of SMGs from Chapman et al. (2005), Coppin et al. (2008) and Kovács et al. (2006) with more local galaxies from Dunne et al. (2000) and local ULIRGs Clements et al. (2010b) confirms this effect. Claims have been made that sources selected at longer wavelengths than the 60 $\mu$m typical of IRAS derived samples (e.g., Symeonidis et al. 2009; Patel et al., in prep.) show less of a separation between the local sources and the higher redshift SMGs. Much of this work is hampered by the poor sampling of the dust SEDs of local objects at wavelengths between 100 and 850 $\mu$m. Recent results from *Herschel* (Amblard et al. 2010) and BLAST (Dye et al. 2009) have begun to fill the gap between local IRAS galaxies and the

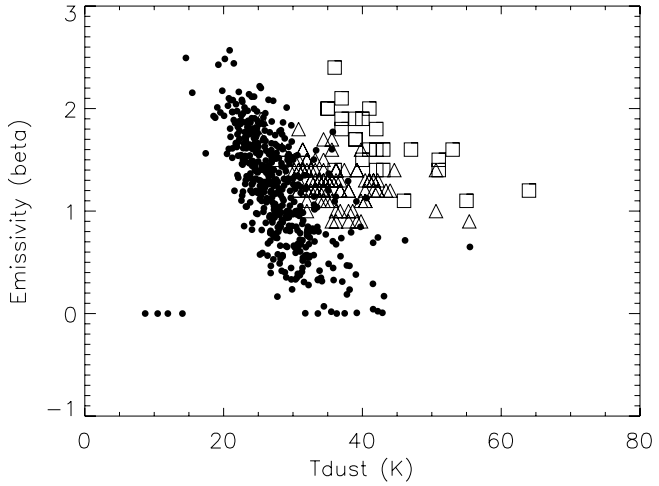


**Fig. 7.** Temperature-$\beta$ correlation for ERCSC-IIFSCz matched galaxies (solid dots) together with data from Dunne et al. (2000) and Clements et al. (2010b) for SCUBA observed sources (triangles and squares respectively). The four sources with $\beta = 0$ and $T < 10$ K at the left of the diagram are the non-thermal dominated sources 3C 279, 0537-441, OJ+287 and 3C 273.

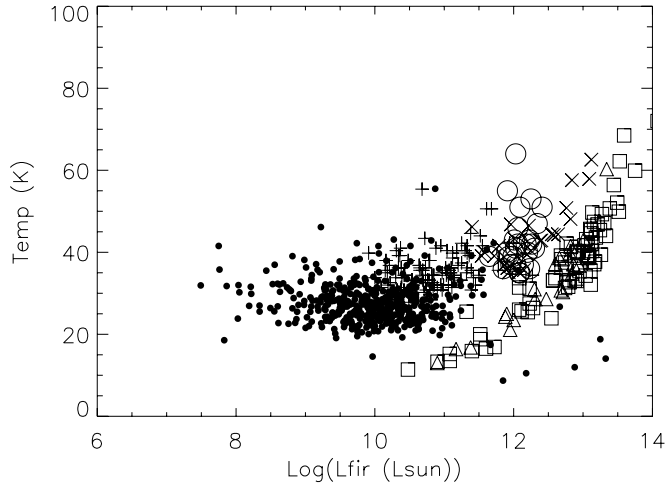


**Fig. 8.** The Temperature-Luminosity plane showing a variety of FIR populations. Open squares are SMGs from Chapman et al. (2005), open triangles are SMGs observed with SHARCII by Coppin et al. (2008) and Kovács et al. (2006). + signs are the SLUGS sources from Dunne et al. (2000), × are intermediate redshift ULIRGs from Yang et al. (2007), ULIRGs from Clements et al. (2010b) are open circles. *Planck*-ERCSC-IIFSCz galaxies are shown as solid dots. As can be seen the previous apparent distinction between the local FIR populations and the SMGs is weakened by sources from this work lying in the same region as the SMGs and by filling in some of the gap between the populations. The four aberrant sources with $T < 15$ K and high $L$ in *the bottom right of the plot* are the non-thermal dominated sources 3C 279, 0537-441, OJ+287 and 3C 273.

SMGs, suggesting that our view of dust temperatures in local objects are biased to warmer temperatures through our dependence on IRAS flux densities. In Fig. 8 we show the positions of *Planck* galaxies on the $L - T$ plane, where the far-IR luminosity is calculated by integrating the luminosity of the fitted dust SED over the range 8–1000 $\mu$m. As can be seen, the gap between the local galaxies and the SMGs is starting to be filled by the *Planck* objects. The *Planck* fluxes for one of these sources may include some contamination from cirrus, but the rest lie in areas of normal to low Galactic cirrus noise and should thus be fully reliable. The large area coverage of *Planck* is particularly important in this as it allows us to probe generic L/ULIRG-class objects ($L_{\rm FIR} > 10^{11}\ L_{\odot}$) rather than having to rely on pre-selected IRAS bright sources as in Clements et al. (2010b). *Herschel* observations, which are also beginning to show the gap being filled, do not yet cover enough area to include many such L/ULRG objects in the local Universe (Amblard et al. 2010). We find several cool ($T < 30$ K) ULIRGs that have very similar characteristics to SMGs. The issue of the apparent distinction between local galaxies and the high-$z$ SMG population thus seems to be approaching resolution.

While the temperature distribution of our objects is consistent with what has been seen elsewhere, we find that some of our galaxies have $\beta$ more than $3\sigma$ less than 1. One possible cause for this might be the 353 GHz flux density being affected by Eddington bias (see e.g., Teerikorpi 2004), leading to "flux-boosting" of lower significance detections, since we accept these fluxes down to $3\sigma$. This is tested by repeating the fits using only the IRAS, 857 and 545 GHz flux densities. While there are small differences in fits to individual objects resulting from the exclusion of the 353 GHz flux densities, the general distribution remains the same, complete with the low $\beta$ sources. We thus conclude that this is a real effect and not due to Eddington bias or any other issue related to the 353 GHz flux densities, such as contamination by emission from the CO 3–2 molecular line. While such low $\beta$ values are not expected in simple models of dust, it is suggestive that the SEDs can be better fit by a parameterization that uses a mixture of dust at two temperatures, as suggested by Dunne & Eales (2001) and which is a good fit to our own galaxy as seen by COBE (Reach et al. 1995). We investigate this by applying two component fits to the dust SEDs.

#### 4.2.2. Two temperature fits

We carry out two temperature component fits on our sources, assuming $\beta = 2$ for both components, and present the temperature-temperature plot in Fig. 9. We also use the Baysian evidence calculated during the fitting process (Jaffe 1996; Jaynes 2003) to determine how many of our sources show evidence for a two component fit above that of the single component $(T, \beta)$ fit. We find that the two component fit is favoured in most cases, with 425 objects giving a higher evidence for this model and only 43 preferring the single component fit. Once again we test the possibility that issues with the lower significance 353 GHz flux densities might bias these fits by repeating the analysis with these fluxes excluded. While this increases the uncertainties in the fits, as with the $(T, \beta)$ fits we find that the exclusion of the 353 GHz fluxes makes no systematic difference to the temperatures found. We find clear evidence for a second dust temperature component in most of the objects in the sample, with a mean $T_{\rm cold} = 16 \pm 4$ K and $T_{\rm warm} = 36 \pm 9$ K.

We find 17 galaxies fit by models containing a dust component with temperatures as low as 10 K. Four of these are the bright blazars and are thus dominated by non-thermal emission, while one is a source that might still contain some cirrus contamination. We thus find at least 13 galaxies which appear to contain very cold dust. Such dust has previously been found in our own galaxy (e.g. Reach et al. 1995), has been suggested in a small number of dwarf galaxies (Galliano et al. 2005; Galametz et al. 2009) and in a small number of spiral galaxies observed by SCUBA (Stevens et al. 2005). The current work is the first time it has been seen before in a large scale extragalactic survey.

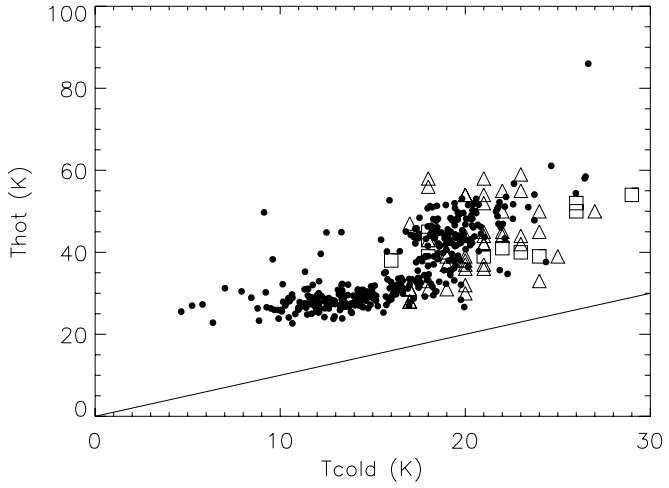


**Fig. 9.** The Temperature-Temperature plane for two temperature component fits for ERCSC-IIFSCz matched galaxies. together with data from Dunne & Eales (2001) and Clements et al. (2010b) for SCUBA observed sources (triangles and squares respectively). Only those ERCSC-IIFSCz sources where the two temperature model is preferred and with a reliably determined cold dust component temperature (i.e., $T/\sigma(T) > 4$) are plotted. The sources with the coldest $T_{\rm cold} < 7$ K in this plot are dominated by non-thermal emission.

Other explanations for these "submm excess" sources have been suggested, especially in the context of low metallicity galaxies where changes in the emissivity as a function of wavelength have been suggested. The small number of sources which have $T_{\rm cold}$ lower than 7 K are all dominated by nonthermal emission. The details of the temperature-temperature plot in Fig. 9, with small scatter and the temperature of the hot component being largely independent of that of the cold component up to $T_{\rm cold} \sim 18$ K will likely have implications concerning the relationship between hot and cold dust components.

### 4.3. The broader ERCSC-IIFSCz sample

The parametric fitting reported here only concerns the 468 non-extended ERCSC-IIFSCz matched galaxies which are detected at $5\sigma$ or greater in the 857 and 545 GHz bands and at $3\sigma$ or greater at 353 GHz. This ensures that uncertainties in the fluxes do not preclude a good fit to the SED, but brings the risk that we might be missing a significantly different subclass of object in the remaining 1122. We have thus applied our fitting methods to this whole sample, regardless of ERCSC S/N beyond the basic detection requirement of a $5\sigma$ or greater detection at 857 GHz. While there are larger errors bars on the fitted parameters we find no indication that galaxies in this larger sample have a different range of dust properties to those discussed above.

## 5. Physical models: template fitting

The FIR and submm spectral energy distributions of galaxies from the IRAS, ISO and *Spitzer* surveys have been successfully modelled with a small number of templates (Rowan-Robinson 1992; Rowan-Robinson et al. 2005; Rowan-Robinson et al. 2008). However the submm data available in such studies is quite limited and we expect to get a much better understanding of cool dust in galaxies with the data from *Planck*. Already with *Herschel*, there is evidence for unexpected quantities of cold dust in some galaxies Rowan-Robinson et al. (2010).

The Rowan-Robinson et al. (2010) study of the SEDs of *Herschel*-detected galaxies used SPIRE flux densities extending from 250 to 500 $\mu$m combined with pre-existing data from SWIRE at *Spitzer* and optical wavelengths. Through the combination of *Planck* data with the IIFSCz, the galaxy sample considered here includes data from the optical to IRAS fluxes, and then the *Planck* data has flux densities at 350, 550 and 850 $\mu$m (857, 545 and 353 GHz). Some of our objects are also detected at 1.4 mm (217 GHz) which is included in our analysis if available. The range of wavelengths available with the ERCSC-IIFSCz sample is thus broader than that available through *Herschel*. This enables us to place better constraints on the role and importance of cold dust in these objects. Our sample is also much larger than the 68 objects considered in Rowan-Robinson et al. (2010), so we can better determine the variety and overall statistics of the SEDs of local galaxies.

The templates used in fitting IRAS (Rowan-Robinson 1992), ISO (Rowan-Robinson et al. 2004) and *Spitzer* (Rowan-Robinson et al. 2008), data are (1) a cirrus (optically thin interstellar dust) model characterised by a radiation intensity $\phi = I(\text{galaxy})/I(\text{ISRF}) = 5$, where I(ISRF) is the intensity of the radiation field in the solar neighbourhood; (2) an M 82-like starburst; (3) a higher optical depth Arp220-like starburst; (4) an AGN dust torus. In fitting the SEDs of *Herschel* galaxies, Rowan-Robinson et al. (2010) use two further cirrus templates with $\phi = 1$ and 0.1, which correspond to significantly cooler dust than in the standard cirrus template. The starting point for the present analysis is the template fit for each object given in the IIFSCz Catalogue (Wang & Rowan-Robinson 2009) and discussed in Wang & Rowan-Robinson (2010). This was done by fitting the optical and near-IR fluxes with an optical galaxy or QSO template. The IRAS data were then fitted with one of the original four Rowan-Robinson et al. (2008) templates. This model is then compared to the *Planck* data. In almost all cases additional components are needed, since the IRAS-based predictions underestimate the submm flux densities provided by *Planck*. The fits are not always good at 353 and 217GHz. This may be a combination of Eddington bias due to the poorer signal-to-noise at this frequency, or CO contamination.

### 5.1. Results from template fits

In Fig. 10 we analyze the SEDs of the archetypal nearby galaxies, M 51, M 100, M 2 and Arp 220. M 51 and M 100 are modelled with two cirrus templates with $\phi = 1$ (solar neighbourhood) and 5 (Galactic Centre), and with a modest M 82 starburst component. M 82 itself needs an additional component of cool cirrus ($\phi = 1$) as well as the M 82 template of Efstathiou and Rowan-Robinson (Efstathiou & Rowan-Robinson 2003). Finally Arp220 is modelled extremely well over all infrared and submm wavelengths by the Arp220 template used by Efstathiou and Rowan-Robinson. The models for these galaxies by Silva et al. (1998) are also shown and perform well, especially for M51 and Arp 220.

Figure 11 shows fits to galaxies with detections in 16 photometric bands: 5 optical bands (SDSS), 3 near infrared bands (2MASS), 4 mid and FIR bands (IRAS) and 4 submm bands (*Planck*). The blue curve is the solar neighbourhood cirrus template ($\phi = 1$) and contributes significantly to the SEDs of 7 out of the 8 galaxies. Dust grains in this component are in the range 15–20 K, depending on grain radius and type (Rowan-Robinson 1992). Dust masses are in the range $10^7$–$3 \times 10^8$ $M_\odot$.

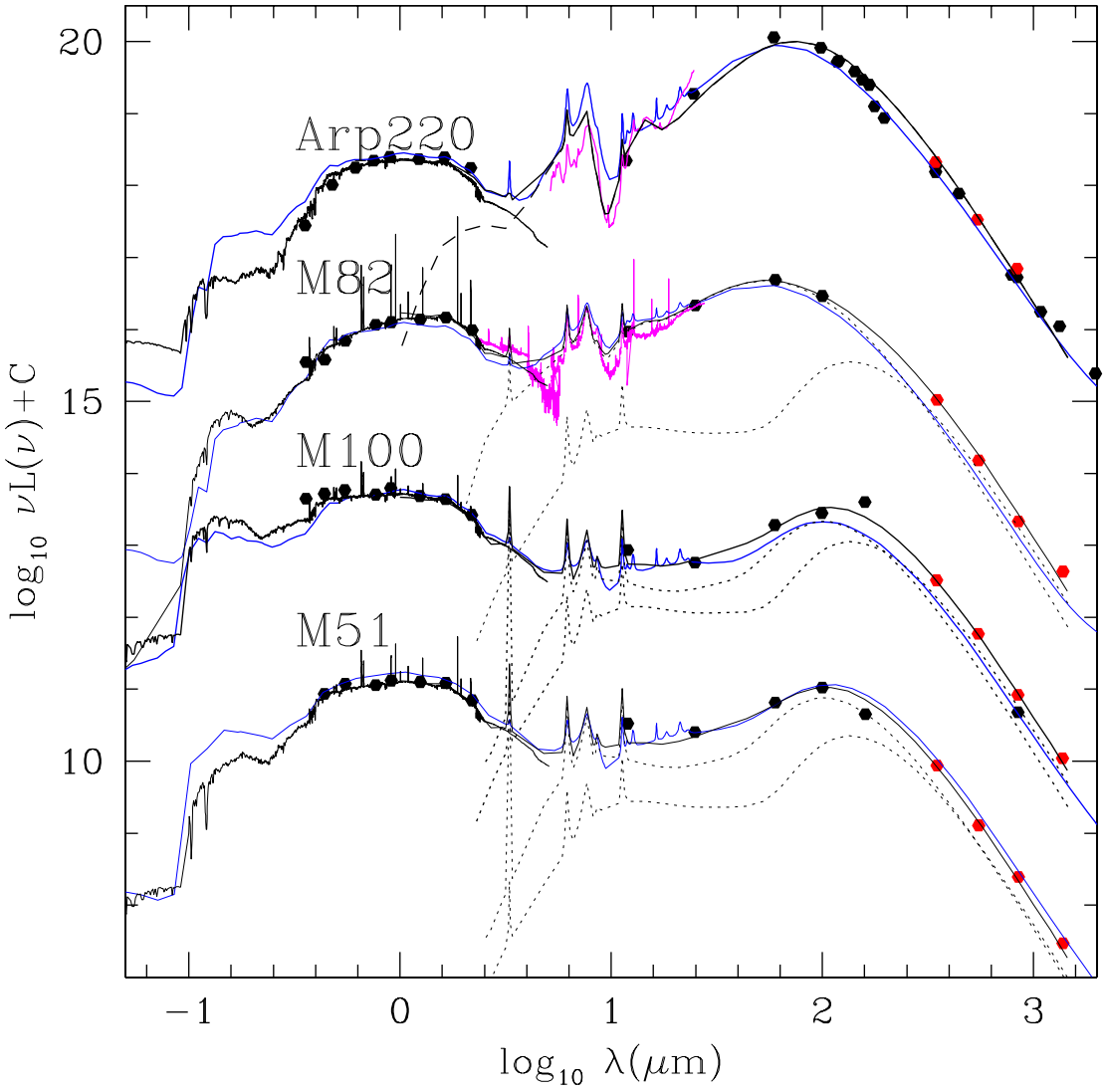


**Fig. 10.** Template fits for the four archetypal nearby galaxies, M 51, M 100, M 82 and Arp 220. Black curves: fits with Efstathiou and Rowan-Robinson templates (black, separate components as dotted lines), blue curves: Silva et al. (1998) models. *Planck* ERCSC data shown as red filled hexagrams. ISO-SWS mid-infrared spectroscopy data for M 82 and *Spitzer*-IRS data for Arp 220 (Siebenmorgen & Krügel 2007) are shown in magenta.

To get an overview of the whole sample, Fig. 12 shows the distribution of 545 GHz (550 $\mu$m) flux density versus redshift for galaxies well detected at 350–850 $\mu$m, and with spectroscopic redshifts. The loci of galaxies with an Arp 220 template at luminosity $L_{\rm IR} = 10^{12}$ and $10^{13}$ $L_\odot$ are shown. With the restrictions to point-sources with good detections in the three highest frequency *Planck* bands, and to galaxies with spectroscopic redshifts, a number of ULIRGs are found in the ERCSC survey, but no HLIRGs, apart from the quasar 3C 273.

Figure 13 shows the colour-ratio $S_{857}/S_{545}$ (i.e. 350 $\mu$m/550 $\mu$m) versus redshift. Galaxies in the IRAS Bright Galaxy Sample are indicated as red dots. Sources for which $T_2 < 10$ K in the 2-temperature fits discussed above are indicated as blue dots. Sources with $\log_{10}(S_{857}/S_{545}) < 0.4$ represent a novel population of cooler submm sources that have only previously been hinted at (Stevens et al. 2005). This plot also demonstrates a method of selecting galaxies containing cold dust that is complementary to the parametric SED fitting process discussed in Sect. 4. We have modelled all 17 galaxies with cool 857 GHz/545 GHz colours ($\log_{10}(S_{857}/S_{545} < 0.4$), and good optical data (Fig. 14). This list includes four of the galaxies identified as having cold dust on the basis of parametric SED fitting above, the remainder of which do not have the full range of optical data necessary for this approach. Almost all require the very cold cirrus model with $T_{\rm dust} = 10$–13 K, $\phi = 0.1$ (green curves in Fig. 14). Table 1 gives the properties of the galaxies whose SEDs we have modelled in detail. We can summarize the SED modelling shown in Figs. 10, 11 and 14 as follows: (1) most nearby galaxies show evidence for dust at temperatures similar to that seen in the solar neighbourhood ($\phi = 1$), as well as the warmer dust found in IRAS, ISO and *Spitzer* studies; (2) there is a new population of cool submm galaxies with even cooler dust ($\phi = 0.1, T_{\rm dust} = 10$–13 K). This cooler dust is likely to have a more extended spatial distribution then generally assumed for the gas and dust in galaxies.

## 6. Conclusions

Our studies of nearby galaxies detected by *Planck* confirm the presence of cold dust in local galaxies, something that has

**Table 1.** Parameters for *Planck* ERCSC-IIFSCz galaxies with SED fits.

| RA | Dec | FSS | dist | $z_{\rm spect}$ | log (*L*) cirr $\psi = 5$ | log (*L*) cirr $\psi = 1$ | log (*L*) cirr $\psi = 0.1$ | log (*L*) SB | log (*L*) Arp220 | log (*L*) Opt | type | $A_V$ | log ($M_*$) $M_\odot$ | log ($M_{\rm dust}$) $M_\odot$ |
|---|---|---|---|---|---|---|---|---|---|---|---|---|---|---|
| | | | | | | | Template | | | | | | | |
| 202.46930 | 47.19290 | F13277+4727 M51 | 0.1 | 0.001544 | 10.05 | 9.49 | | 9.60 | | 10.35 | Sbc | 0.0 | 10.75 | 7.54 |
| 185.72728 | 15.82777 | F12203+1605 M100 | 0.4 | 0.005240 | 10.53 | 10.19 | | 9.98 | | 11.22 | Sbc | 0.0 | 11.62 | 8.15 |
| 148.97540 | 69.68221 | F09517+6954 M 82 | 0.2 | 0.000677 | | 9.19 | | 10.41 | | 9.95 | E | 0.0 | 10.54 | 7.18 |
| 233.74080 | 23.49795 | F15327+2340 Arp220 | 0.4 | 0.01813 | | | | | 12.15 | 10.58 | E | 0.0 | 11.17 | 8.15 |
| | | | | | | | 16-band, $z < 0.01$ | | | | | | | |
| 175.24310 | 11.47154 | F11383+1144 NGC 3810 | 0.1 | 0.003312 | 9.70 | 9.69 | | 9.24 | | 10.00 | Sab | 0.0 | 10.57 | 7.58 |
| 143.03957 | 21.50516 | F09293+2143 NGC 2903 | 0.2 | 0.001855 | 9.70 | 9.49 | | 9.38 | | 10.41 | Scd | 0.2 | 10.79 | 7.43 |
| 213.89354 | 36.22261 | F14134+3627 NGC 5529 | 0.3 | 0.009591 | | 10.19 | | 9.60 | | 10.70 | Sab | 0.65 | 11.27 | 8.44 |
| 181.50023 | 47.47356 | F12034+4745 NGC 4096 | 0.3 | 0.001888 | 8.90 | 9.09 | | 8.60 | | 9.65 | Sab | 0.6 | 10.22 | 6.95 |
| 206.59677 | 43.86664 | F13443+4407 NGC 5297 | 0.5 | 0.008036 | 9.90 | 9.99 | | | | 10.60 | Scd | 0.4 | 11.04 | 7.86 |
| 184.95674 | 29.61180 | F12173+2953 NGC 4274 | 0.7 | 0.003102 | | 9.64 | | | | 10.40 | Scd | 0.0 | 10.94 | 7.45 |
| 218.18851 | 49.45234 | F14310+4940 NGC 5676 | 0.4 | 0.007052 | 10.60 | | | | | 10.70 | Sab | 0.4 | 11.27 | 7.71 |
| 178.20813 | 44.12143 | F11502+4423 NGC 3938 | 0.5 | 0.002699 | | 9.59 | | 9.10 | | 9.90 | Scd | 0.5 | 10.34 | 7.40 |
| | | | | | | | Cold log ($S_{857}/S_{545}$) < 0.4 | | | | | | | |
| 159.78535 | 41.69160 | F10361+4155 | 2.0 | 0.002228 | | | 8.52 | 8.10 | | 7.50 | sb | 0.2 | 7.52 | 7.33 |
| 179.31494 | 49.28748 | F11547+4933 | 0.4 | 0.002592 | | 8.79 | | | | 8.70 | sb | 0.0 | 8.72 | 6.60 |
| 218.19263 | 9.88910 | F14302+1006 | 0.6 | 0.004574 | 9.40 | | 8.92 | | | 9.60 | Scd | 0.2 | 10.04 | 7.76 |
| 208.22507 | –1.12087 | F13503-0052 | 0.4 | 0.004623 | | 9.64 | | | | 9.70 | Scd | 0.5 | 10.14 | 7.45 |
| 148.79717 | 9.27136 | F09521+0930 | 0.0 | 0.004854 | | | 8.92 | 9.40 | | 9.60 | Scd | 0.0 | 10.04 | 7.73 |
| 219.79150 | 5.25526 | F14366+0534 | 0.4 | 0.005020 | | 9.09 | 8.62 | 8.70 | | 10.35 | Scd | 0.2 | 10.79 | 7.54 |
| 158.12950 | 65.03790 | F10290+6517 | 0.4 | 0.005624 | 9.40 | | 8.62 | | | 9.80 | Scd | 0.2 | 10.24 | 7.48 |
| 210.53130 | 55.79348 | F14004+5603 | 1.4 | 0.006014 | 9.05 | | 8.67 | | | 10.25 | Scd | 0.7 | 10.69 | 7.50 |
| 208.72266 | 41.30995 | F13527+4133 | 0.0 | 0.007255 | 9.51 | 8.40 | | | | 9.96 | Scd | 0.2 | 10.40 | 6.76 |
| 205.57553 | 60.77630 | F13405+6101 | 0.3 | 0.007322 | | 9.20 | 8.63 | | | 9.61 | Sbc | 0.5 | 10.01 | 7.58 |
| 228.37207 | 58.49204 | F15122+5841 | 1.0 | 0.008474 | 9.26 | | 8.95 | | | 9.51 | Scd | 0.15 | 9.95 | 7.77 |
| 231.67357 | 40.55709 | F15248+4044 | 0.4 | 0.008743 | | 9.70 | 9.43 | 9.41 | | 10.16 | Scd | 0.7 | 10.60 | 8.31 |
| 226.95305 | 54.74415 | F15064+5456 | 0.7 | 0.01043 | | 10.00 | | | | 10.16 | Scd | 0.4 | 10.60 | 7.81 |
| 126.57545 | 22.88144 | F08233+2303 | 1.3 | 0.01794 | | 10.20 | 10.13 | | | 9.81 | Scd | 0.3 | 10.25 | 8.99 |
| 231.43570 | 52.44624 | F15243+5237 | 0.3 | 0.01948 | 10.19 | | 9.81 | | | 10.44 | Sab | 0.2 | 11.01 | 8.64 |
| 237.68201 | 55.60954 | F15495+5545 | 0.2 | 0.03974 | 10.55 | | 10.52 | 10.20 | | 10.70 | Sab | 0.0 | 11.27 | 9.34 |
| 66.76954 | –49.12881 | F04257-4913 | 0.8 | 0.05828 | | | 10.62 | 11.55 | | 10.85 | Sab | 0.0 | 11.42 | 9.43 |

**Notes.** Table columns are: ERCSC RA and Dec, IRAS FSC name, separation between ERCSC and IIFSCz position, spectroscopic redshift, luminosity in cirrus $\phi = 5$, $\phi = 1$ and $\phi = 0.1$ components, luminosity in M 82 and Arp220 starburst components, optical luminosity, optical SED type, extinction (additional to that inherent to the individual templates), stellar mass and dust mass. Total far-IR luminosity can be obtained by summing the various different components. Stellar mass and dust mass are calculated as in Rowan-Robinson et al. (2008), where the methods and uncertainties in the derived quantities are discussed in detail. Where the sources have a well known name this is given beneath the IRAS name. All luminosities are measured in solar luminosities.

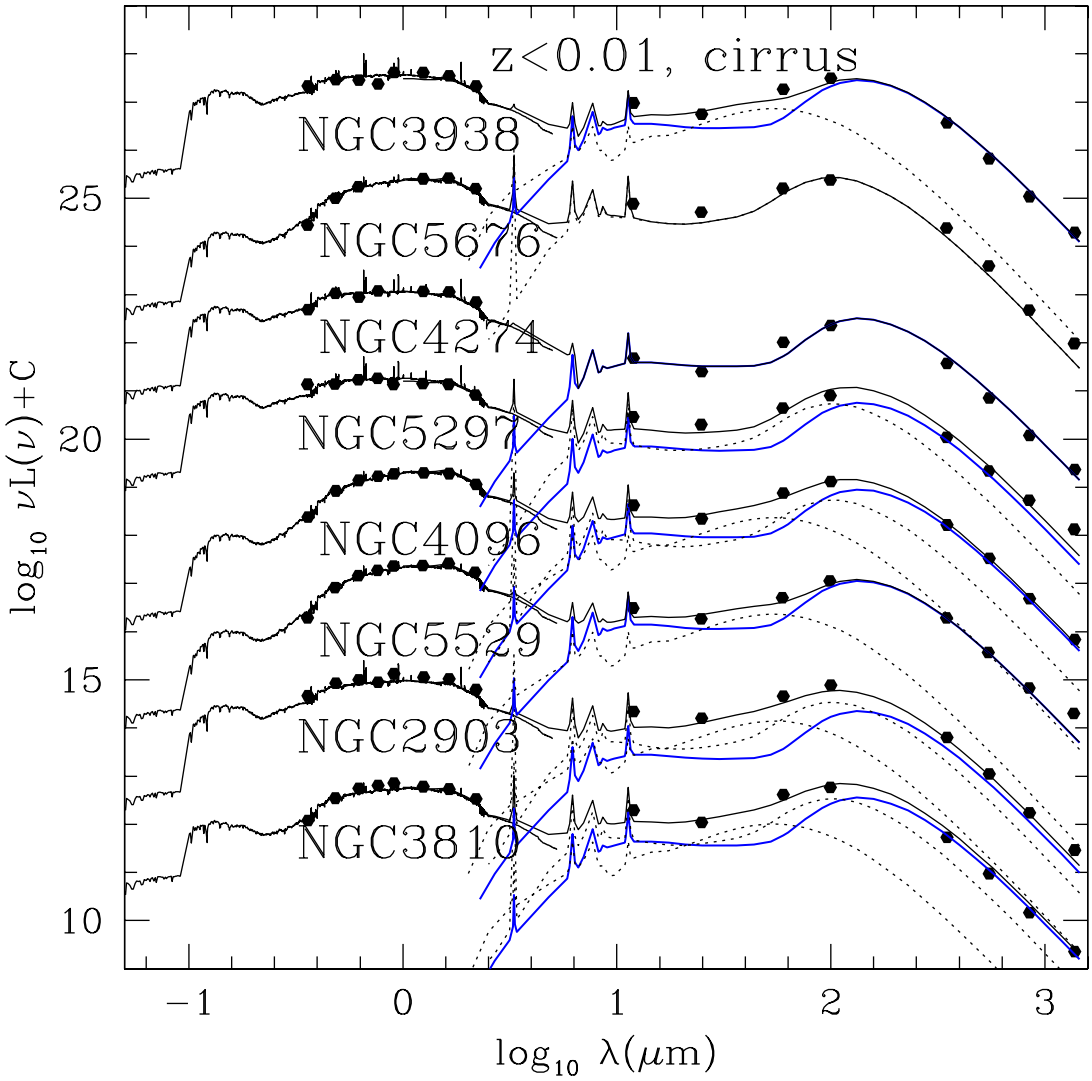


**Fig. 11.** Template fits for 8 nearby galaxies with detections in 16 bands. Blue curve is cirrus template used for solar neighbourhood ($T_{\rm dust}$ = 15–20 K, $\phi$ = 1), other components shown as dotted lines.

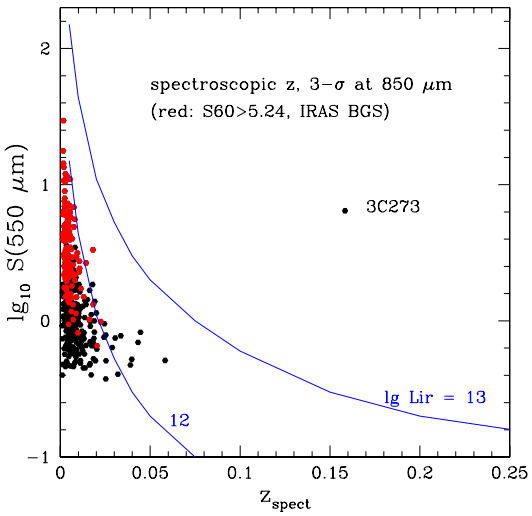


**Fig. 12.** 545 GHz flux density versus redshift, showing loci for Arp220 template with $L_{\rm IR} = 10^{12}$ and $10^{13}$ $L_\odot$. Red dots are those galaxies in the IRAS Bright Galaxy Survey (BGS). We show here that the BGS does not sample as wide a range of galaxy properties as the Planck-IIFSCz sample discussed here.

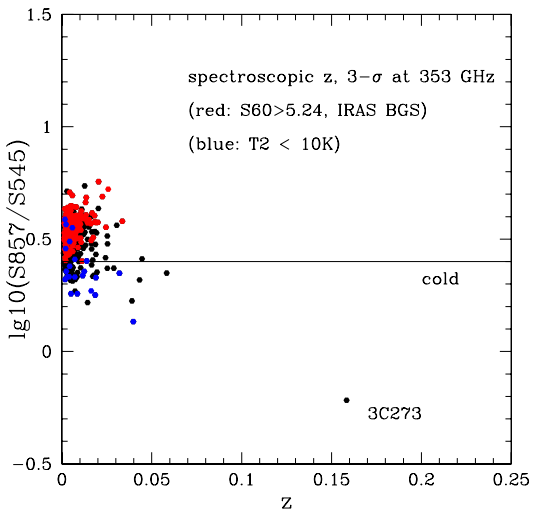


**Fig. 13.** $S_{857}/S_{545}$ colour-ratio versus redshift. Points in red are IRAS BGS sources, points in blue are those sources identified as having $T_2 <$ 10 K on the basis of parametric fits.

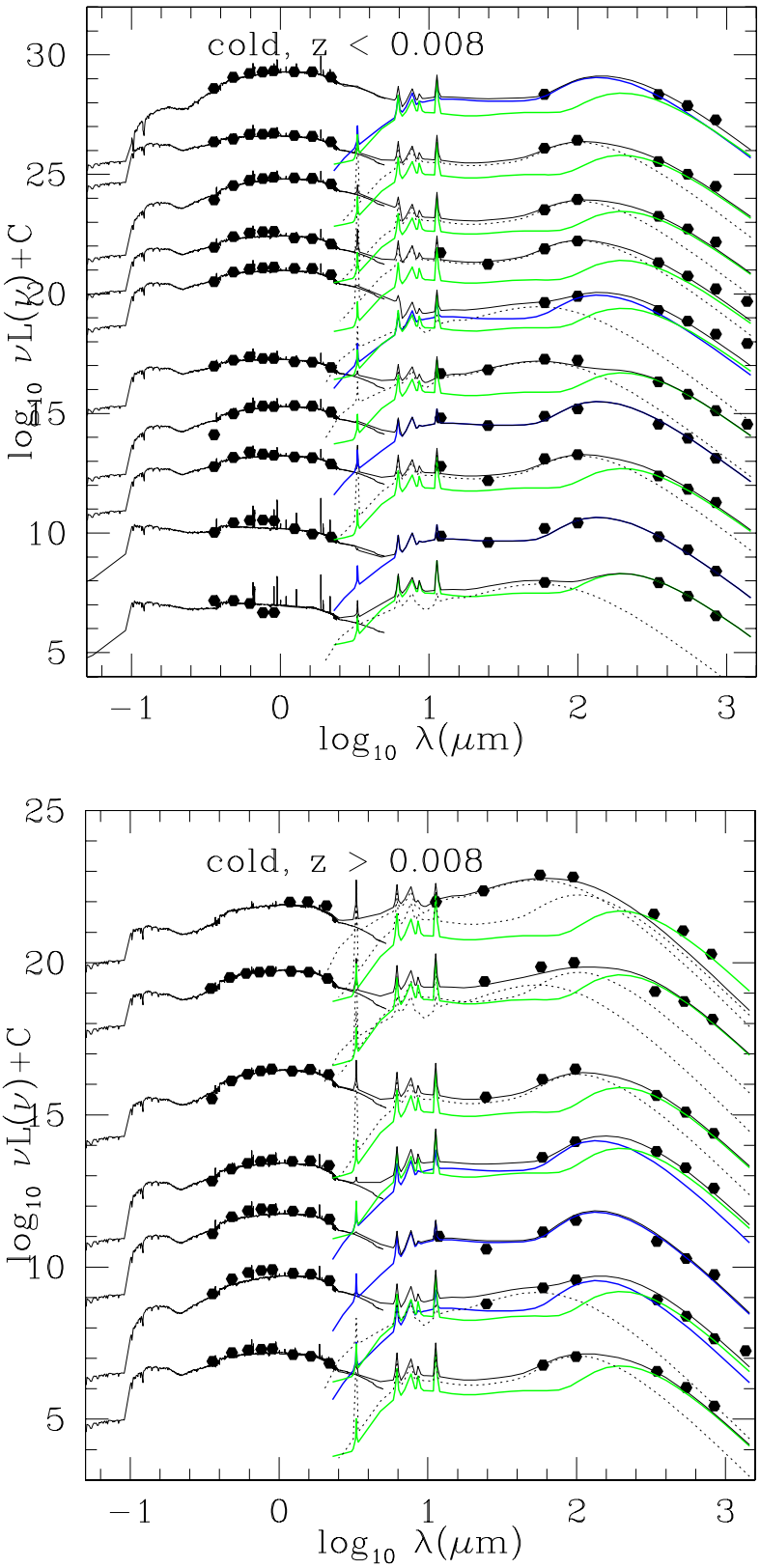


**Fig. 14.** Template fits for cool ERCSC galaxies ($\log_{10}(S_{857}/S_{545}) < 0.4$). Blue curve: cirrus with $\phi = 1$, green curve: cirrus with $\phi = 0.1$.

previously only been hinted at, largely in dwarf galaxies. The temperature of this dust, is similar to that found in the solar neighbourhood. We also find that some local galaxies are both luminous and cool, with properties similar to those of the distant SMGs uncovered in deep submm surveys. This suggests that previous studies of dust in local galaxies have been biased away from such luminous cool objects. We also find that the dust SEDs in most galaxies are better described by parametric models containing two dust components, one warm and one cold, with the cold component reaching temperatures as low as 10 K.

Some objects have SEDs dominated by this cold material. These conclusions are based on both parametric fits and by detailed fitting of radiative transfer derived physical templates to the SEDs. Other physical or parametric descriptions of dust, for example where $\beta$ varies with wavelength, might lead to different results regarding this very cold component. We note in this context, however, that SED fits for galaxies in the H-ATLAS survey are reaching similar conclusions to this study (Smith et al., in prep.). This paper represents the first exploitation of *Planck* data for the study of a large sample of galaxies in the local Universe. As such it indicates both the benefits and hazards of the ERCSC for this work, but it also clearly demonstrates the tremendous potential of *Planck* data for the study of dust in galaxies.

*Acknowledgements.* This research has made use of the NASA/IPAC Extragalactic Database (NED) which is operated by the Jet Propulsion Laboratory, California Institute of Technology, under contract with the National Aeronautics and Space Administration. Use was also made of data from the Sloan Digital Sky Survey (SDSS) and the Two Micron All Sky Survey (2MASS). Funding for the SDSS and SDSS-II has been provided by the Alfred P. Sloan Foundation, the Participating Institutions, the National Science Foundation, the U.S. Department of Energy, the National Aeronautics and Space Administration, the Japanese Monbukagakusho, the Max Planck Society, and the Higher Education Funding Council for England. The SDSS Web Site is http://www.sdss.org/. 2MASS is a joint project of the University of Massachusetts and the Infrared Processing and Analysis Center/California Institute of Technology, funded by the National Aeronautics and Space Administration and the National Science Foundation. The Planck Collaboration acknowledges the support of: ESA; CNES and CNRS/INSU-IN2P3-INP (France); ASI, CNR, and INAF (Italy); NASA and DoE (USA); STFC and UKSA (UK); CSIC, MICINN and JA (Spain); Tekes, AoF and CSC (Finland); DLR and MPG (Germany); CSA (Canada); DTU Space (Denmark); SER/SSO (Switzerland); RCN (Norway); SFI (Ireland); FCT/MCTES (Portugal); and DEISA (EU). A description of the Planck Collaboration and a list of its members, indicating which technical or scientific activities they have been involved in, can be found at http://www.rssd.esa.int/index.php?project=PLANCK\&page=Planck_Collaboration. We thank the anonymous referee for many useful comments that have improved this paper.

## References

Amblard, A., Cooray, A., Serra, P., et al. 2010, A&A, 518, L9
Austermann, J. E., Dunlop, J. S., Perera, T. A., et al. 2010, MNRAS, 401, 160
Bayet, E., Gerin, M., Phillips, T. G., & Contursi, A. 2006, A&A, 460, 467
Bersanelli, M., Mandolesi, N., Butler, R. C., et al. 2010, A&A, 520, A4
Bertin, E., & Arnouts, S. 1996, A&AS, 117, 393
Béthermin, M., Dole, H., Beelen, A., & Aussel, H. 2010, A&A, 512, A78
Boselli, A., Ciesla, L., Buat, V., et al. 2010, A&A, 518, L61
Carvalho, P., Rocha, G., & Hobson, M. P. 2009, MNRAS, 393, 681
Chapman, S. C., Blain, A. W., Smail, I., & Ivison, R. J. 2005, ApJ, 622, 772
Clements, D. L., Bendo, G., Pearson, C., et al. 2010a, MNRAS, 1778
Clements, D. L., Dunne, L., & Eales, S. 2010b, MNRAS, 403, 274
Clements, D. L., Rigby, E., Maddox, S., et al. 2010c, A&A, 518, L8
Coppin, K., Chapin, E. L., Mortier, A. M. J., et al. 2006, MNRAS, 372, 1621
Coppin, K., Halpern, M., Scott, D., et al. 2008, MNRAS, 384, 1597
Dale, D. A., Bendo, G. J., Engelbracht, C. W., et al. 2005, ApJ, 633, 857
Devereux, N. A., & Young, J. S. 1990, ApJ, 359, 42
Devlin, M. J., Ade, P. A. R., Aretxaga, I., et al. 2009, Nature, 458, 737
Dole, H., Gispert, R., Lagache, G., et al. 2001, A&A, 372, 364
Dunne, L., & Eales, S. A. 2001, MNRAS, 327, 697
Dunne, L., Eales, S., Edmunds, M., et al. 2000, MNRAS, 315, 115
Dunne, L., Gomez, H., da Cunha, E., et al. 2011, MNRAS, 417, 1510
Dye, S., Ade, P. A. R., Bock, J. J., et al. 2009, ApJ, 703, 285
Dye, S., Dunne, L., Eales, S., et al. 2010, A&A, 518, L10
Eales, S., Lilly, S., Webb, T., et al. 2000, AJ, 120, 2244
Eales, S., Dunne, L., Clements, D., et al. 2010a, PASP, 122, 499
Eales, S. A., Raymond, G., Roseboom, I. G., et al. 2010b, A&A, 518, L23
Efstathiou, A., & Rowan-Robinson, M. 2003, MNRAS, 343, 322
Fixsen, D. J., Dwek, E., Mather, J. C., Bennett, C. L., & Shafer, R. A. 1998, ApJ, 508, 123
Frayer, D. T., Fadda, D., Yan, L., et al. 2006, AJ, 131, 250
Galametz, M., Madden, S., Galliano, F., et al. 2009, A&A, 508, 645
Galliano, F., Madden, S. C., Jones, A. P., Wilson, C. D., & Bernard, J. 2005, A&A, 434, 867
Gispert, R., Lagache, G., & Puget, J. L. 2000, A&A, 360, 1
Hughes, D. H., Serjeant, S., Dunlop, J., et al. 1998, Nature, 394, 241
Jaffe, A. 1996, ApJ, 471, 24
Jaynes, E. 2003, Probability Theory: the Logic of Science (Cambridge University Press)
Kovács, A., Chapman, S. C., Dowell, C. D., et al. 2006, ApJ, 650, 592
Lamarre, J., Puget, J., Ade, P. A. R., et al. 2010, A&A, 520, A9
Leahy, J. P., Bersanelli, M., D'Arcangelo, O., et al. 2010, A&A, 520, A8
Lewis, A., & Bridle, S. 2002, Phys. Rev. D, 66, 103511
Mandolesi, N., Bersanelli, M., Butler, R. C., et al. 2010, A&A, 520, A3
Mennella, A., Bersanelli, M., Butler, R. C., et al. 2011, A&A, 536, A3
Odenwald, S., Newmark, J., & Smoot, G. 1996 [arXiv:astro-ph/9610238]
Oliver, S. J., Wang, L., Smith, A. J., et al. 2010, A&A, 518, L21
Planck Collaboration 2011a, A&A, 536, A1
Planck Collaboration 2011b, A&A, 536, A2
Planck Collaboration 2011c, A&A, 536, A7
Planck Collaboration 2011d, A&A, 536, A8
Planck Collaboration 2011e, A&A, 536, A9
Planck Collaboration 2011f, A&A, 536, A10
Planck Collaboration 2011g, A&A, 536, A11
Planck Collaboration 2011h, A&A, 536, A12
Planck Collaboration 2011i, A&A, 536, A13
Planck Collaboration 2011j, A&A, 536, A14
Planck Collaboration 2011k, A&A, 536, A15
Planck Collaboration 2011l, A&A, 536, A16
Planck Collaboration 2011m, A&A, 536, A17
Planck Collaboration 2011n, A&A, 536, A18
Planck Collaboration 2011o, A&A, 536, A19
Planck Collaboration 2011p, A&A, 536, A20
Planck Collaboration 2011q, A&A, 536, A21
Planck Collaboration 2011r, A&A, 536, A22
Planck Collaboration 2011s, A&A, 536, A23
Planck Collaboration 2011t, A&A, 536, A24
Planck Collaboration 2011u, A&A, 536, A25
Planck Collaboration 2011v, The Explanatory Supplement to the Planck Early Release Compact Source Catalogue (ESA)
Planck Collaboration 2011w, A&A, 536, A26
Planck HFI Core Team 2011a, A&A, 536, A4
Planck HFI Core Team 2011b, A&A, 536, A6
Puget, J., Abergel, A., Bernard, J., et al. 1996, A&A, 308, L5
Reach, W. T., Dwek, E., Fixsen, D. J., et al. 1995, ApJ, 451, 188
Rosset, C., Tristram, M., Ponthieu, N., et al. 2010, A&A, 520, A13
Rowan-Robinson, M. 1992, MNRAS, 258, 787
Rowan-Robinson, M., Lari, C., Perez-Fournon, I., et al. 2004, MNRAS, 351, 1290
Rowan-Robinson, M., Babbedge, T., Surace, J., et al. 2005, AJ, 129, 1183
Rowan-Robinson, M., Babbedge, T., Oliver, S., et al. 2008, MNRAS, 386, 697
Rowan-Robinson, M., Roseboom, I. G., Vaccari, M., et al. 2010, MNRAS, 409, 2
Schlegel, D. J., Finkbeiner, D. P., & Davis, M. 1998, ApJ, 500, 525
Seaquist, E., Yao, L., Dunne, L., & Cameron, H. 2004, MNRAS, 349, 1428
Siebenmorgen, R., & Krügel, E. 2007, A&A, 461, 445
Silva, L., Granato, G. L., Bressan, A., & Danese, L. 1998, ApJ, 509, 103
Skrutskie, M. F., Cutri, R. M., Stiening, R., et al. 2006, AJ, 131, 1163
Smail, I., Ivison, R. J., & Blain, A. W. 1997, ApJ, 490, L5
Stevens, J. A., Amure, M., & Gear, W. K. 2005, MNRAS, 357, 361
Symeonidis, M., Page, M. J., Seymour, N., et al. 2009, MNRAS, 397, 1728
Tauber, J. A., Mandolesi, N., Puget, J., et al. 2010, A&A, 520, A1
Teerikorpi, P. 2004, A&A, 424, 73
Vlahakis, C., Dunne, L., & Eales, S. 2005, MNRAS, 364, 1253
Wang, L., & Rowan-Robinson, M. 2009, MNRAS, 398, 109
Wang, L., & Rowan-Robinson, M. 2010, MNRAS, 401, 35
Weiß, A., Kovács, A., Coppin, K., et al. 2009, ApJ, 707, 1201
Willmer, C. N. A., Rieke, G. H., Le Floc'h, E., et al. 2009, AJ, 138, 146
Yang, M., Greve, T. R., Dowell, C. D., & Borys, C. 2007, ApJ, 660, 1198
York, D. G., Adelman, J., Anderson, Jr., J. E., et al. 2000, AJ, 120, 1579
Zacchei, A., Maino, D., Baccigalupi, C., et al. 2011, A&A, 536, A5

[1] Aalto University Metsähovi Radio Observatory, Metsähovintie 114, 02540 Kylmälä, Finland
[2] Agenzia Spaziale Italiana Science Data Center, c/o ESRIN, via Galileo Galilei, Frascati, Italy

[3] Astroparticule et Cosmologie, CNRS (UMR7164), Université Denis Diderot Paris 7, Bâtiment Condorcet, 10 rue A. Domon et Léonie Duquet, Paris, France
[4] Astrophysics Group, Cavendish Laboratory, University of Cambridge, J J Thomson Avenue, Cambridge CB3 0HE, UK
[5] Atacama Large Millimeter/submillimeter Array, ALMA Santiago Central Offices, Alonso de Cordova 3107, Vitacura, Casilla 763 0355, Santiago, Chile
[6] CITA, University of Toronto, 60 St. George St., Toronto, ON M5S 3H8, Canada
[7] CNRS, IRAP, 9 Av. Colonel Roche, BP 44346, 31028 Toulouse Cedex 4, France
[8] California Institute of Technology, Pasadena, California, USA
[9] DAMTP, University of Cambridge, Centre for Mathematical Sciences, Wilberforce Road, Cambridge CB3 0WA, UK
[10] DSM/Irfu/SPP, CEA-Saclay, 91191 Gif-sur-Yvette Cedex, France
[11] DTU Space, National Space Institute, Juliane Mariesvej 30, Copenhagen, Denmark
[12] Departamento de Física, Universidad de Oviedo, Avda. Calvo Sotelo s/n, Oviedo, Spain
[13] Department of Astronomy and Astrophysics, University of Toronto, 50 Saint George Street, Toronto, Ontario, Canada
[14] Department of Physics & Astronomy, University of British Columbia, 6224 Agricultural Road, Vancouver, British Columbia, Canada
[15] Department of Physics, Gustaf Hällströmin katu 2a, University of Helsinki, Helsinki, Finland
[16] Department of Physics, Princeton University, Princeton, New Jersey, USA
[17] Department of Physics, Purdue University, 525 Northwestern Avenue, West Lafayette, Indiana, USA
[18] Department of Physics, University of California, Berkeley, California, USA
[19] Department of Physics, University of California, One Shields Avenue, Davis, California, USA
[20] Department of Physics, University of California, Santa Barbara, California, USA
[21] Department of Physics, University of Illinois at Urbana-Champaign, 1110 West Green Street, Urbana, Illinois, USA
[22] Dipartimento di Fisica G. Galilei, Università degli Studi di Padova, via Marzolo 8, 35131 Padova, Italy
[23] Dipartimento di Fisica, Università La Sapienza, P. le A. Moro 2, Roma, Italy
[24] Dipartimento di Fisica, Università degli Studi di Milano, via Celoria, 16, Milano, Italy
[25] Dipartimento di Fisica, Università degli Studi di Trieste, via A. Valerio 2, Trieste, Italy
[26] Dipartimento di Fisica, Università di Ferrara, via Saragat 1, 44122 Ferrara, Italy
[27] Dipartimento di Fisica, Università di Roma Tor Vergata, via della Ricerca Scientifica, 1, Roma, Italy
[28] Discovery Center, Niels Bohr Institute, Blegdamsvej 17, Copenhagen, Denmark
[29] Dpto. Astrofísica, Universidad de La Laguna (ULL), 38206 La Laguna, Tenerife, Spain
[30] European Southern Observatory, ESO Vitacura, Alonso de Cordova 3107, Vitacura, Casilla 19001, Santiago, Chile
[31] European Space Agency, ESAC, Planck Science Office, Camino bajo del Castillo, s/n, Urbanización Villafranca del Castillo, Villanueva de la Cañada, Madrid, Spain
[32] European Space Agency, ESTEC, Keplerlaan 1, 2201 AZ Noordwijk, The Netherlands
[33] Haverford College Astronomy Department, 370 Lancaster Avenue, Haverford, Pennsylvania, USA
[34] Helsinki Institute of Physics, Gustaf Hällströmin katu 2, University of Helsinki, Helsinki, Finland
[35] INAF – Osservatorio Astrofisico di Catania, via S. Sofia 78, Catania, Italy
[36] INAF – Osservatorio Astronomico di Padova, Vicolo dell'Osservatorio 5, Padova, Italy
[37] INAF – Osservatorio Astronomico di Roma, via di Frascati 33, Monte Porzio Catone, Italy
[38] INAF – Osservatorio Astronomico di Trieste, via G.B. Tiepolo 11, Trieste, Italy
[39] INAF/IASF Bologna, via Gobetti 101, Bologna, Italy
[40] INAF/IASF Milano, via E. Bassini 15, Milano, Italy
[41] INRIA, Laboratoire de Recherche en Informatique, Université Paris-Sud 11, Bâtiment 490, 91405 Orsay Cedex, France
[42] IPAG: Institut de Planétologie et d'Astrophysique de Grenoble, Université Joseph Fourier, Grenoble 1/CNRS-INSU, UMR 5274, 38041 Grenoble, France
[43] ISDC Data Centre for Astrophysics, University of Geneva, ch. d'Ecogia 16, Versoix, Switzerland
[44] Imperial College London, Astrophysics group, Blackett Laboratory, Prince Consort Road, London, SW7 2AZ, UK
[45] Infrared Processing and Analysis Center, California Institute of Technology, Pasadena, CA 91125, USA
[46] Institut Néel, CNRS, Université Joseph Fourier Grenoble I, 25 rue des Martyrs, Grenoble, France
[47] Institut d'Astrophysique Spatiale, CNRS (UMR 8617) Université Paris-Sud 11, Bâtiment 121, Orsay, France
[48] Institut d'Astrophysique de Paris, CNRS UMR 7095, Université Pierre & Marie Curie, 98bis boulevard Arago, Paris, France
[49] Institute of Astronomy and Astrophysics, Academia Sinica, Taipei, Taiwan
[50] Institute of Astronomy, University of Cambridge, Madingley Road, Cambridge CB3 0HA, UK
[51] Institute of Theoretical Astrophysics, University of Oslo, Blindern, Oslo, Norway
[52] Instituto de Astrofísica de Canarias, C/Vía Láctea s/n, La Laguna, Tenerife, Spain
[53] Instituto de Física de Cantabria (CSIC-Universidad de Cantabria), Avda. de los Castros s/n, Santander, Spain
[54] Jet Propulsion Laboratory, California Institute of Technology, 4800 Oak Grove Drive, Pasadena, California, USA
[55] Jodrell Bank Centre for Astrophysics, Alan Turing Building, School of Physics and Astronomy, The University of Manchester, Oxford Road, Manchester, M13 9PL, UK
[56] Kavli Institute for Cosmology Cambridge, Madingley Road, Cambridge, CB3 0HA, UK
[57] LERMA, CNRS, Observatoire de Paris, 61 avenue de l'Observatoire, Paris, France
[58] Laboratoire AIM, IRFU/Service d'Astrophysique – CEA/DSM – CNRS – Université Paris Diderot, Bât. 709, CEA-Saclay, 91191 Gif-sur-Yvette Cedex, France
[59] Laboratoire Traitement et Communication de l'Information, CNRS (UMR 5141) and Télécom ParisTech, 46 rue Barrault, 75634 Paris Cedex 13, France
[60] Laboratoire de Physique Subatomique et de Cosmologie, CNRS/IN2P3, Université Joseph Fourier Grenoble I, Institut National Polytechnique de Grenoble, 53 rue des Martyrs, 38026 Grenoble Cedex, France
[61] Laboratoire de l'Accélérateur Linéaire, Université Paris-Sud 11, CNRS/IN2P3, Orsay, France
[62] Lawrence Berkeley National Laboratory, Berkeley, California, USA
[63] Max-Planck-Institut für Astrophysik, Karl-Schwarzschild-Str. 1, 85741 Garching, Germany
[64] MilliLab, VTT Technical Research Centre of Finland, Tietotie 3, Espoo, Finland
[65] National University of Ireland, Department of Experimental Physics, Maynooth, Co. Kildare, Ireland
[66] Niels Bohr Institute, Blegdamsvej 17, Copenhagen, Denmark
[67] Observational Cosmology, Mail Stop 367-17, California Institute of Technology, Pasadena, CA, 91125, USA
[68] Optical Science Laboratory, University College London, Gower Street, London, UK

[69] SISSA, Astrophysics Sector, via Bonomea 265, 34136, Trieste, Italy
[70] SUPA, Institute for Astronomy, University of Edinburgh, Royal Observatory, Blackford Hill, Edinburgh EH9 3HJ, UK
[71] School of Physics and Astronomy, Cardiff University, Queens Buildings, The Parade, Cardiff, CF24 3AA, UK
[72] Space Sciences Laboratory, University of California, Berkeley, California, USA
[73] Stanford University, Dept of Physics, Varian Physics Bldg, 382 via Pueblo Mall, Stanford, California, USA
[74] Université de Toulouse, UPS-OMP, IRAP, 31028 Toulouse Cedex 4, France
[75] Universities Space Research Association, Stratospheric Observatory for Infrared Astronomy, MS 211-3, Moffett Field, CA 94035, USA
[76] University of Granada, Departamento de Física Teórica y del Cosmos, Facultad de Ciencias, Granada, Spain
[77] University of Miami, Knight Physics Building, 1320 Campo Sano Dr., Coral Gables, Florida, USA
[78] Warsaw University Observatory, Aleje Ujazdowskie 4, 00-478 Warszawa, Poland